Design and characterization of methods and biological components to realize synthetic neurotransmission

by

Catherine McKenzie

August, 2018

A thesis presented to the
Graduate School
of the
Institute of Science and Technology Austria, Klosterneuburg, Austria
in partial fulfillment of the requirements
for the degree of
Doctor of Philosophy

The dissertation of Catherine McKenzie, titled *"Design and characterization of methods and biological components to realize synthetic neurotransmission"*, is approved by:

Supervisor: Dr. Harald Janovjak, IST Austria, Klosterneuburg, Austria

Signature: _____

Committee Member: Dr. Simon Hippenmeyer, IST Austria, Klosterneuburg, Austria

Signature: _____

Committee Member: Dr. Harald Sitte, Medical University of Vienna, Center for Physiology and Pharmacology, Institute of Pharmacology, Vienna, Austria

Signature: _____

Exam Chair: Dr. Florian Schur, IST Austria, Klosterneuburg, Austria

Signature: _____

I hereby declare that this dissertation is my own work and that it does not contain other people's work without this being so stated; this thesis does not contain my previous work without this being stated, and the bibliography contains all the literature that I used in writing the dissertation.

I declare that this is a true copy of my thesis, including any final revisions, as approved by my thesis committee, and that this thesis has not been submitted for a higher degree to any other university or institution.

I certify that any republication of materials presented in this thesis has been approved by the relevant publishers and co-authors.

Signature: _____

Catherine McKenzie

October 31, 2018

Abstract

A major challenge in neuroscience research is to dissect the circuits that orchestrate behavior in health and disease. Proteins from a wide range of non-mammalian species, such as microbial opsins, have been successfully transplanted to specific neuronal targets to override their natural communication patterns. The goal of our work is to manipulate synaptic communication in a manner that closely incorporates the functional intricacies of synapses by preserving temporal encoding (i.e. the firing pattern of the presynaptic neuron) and connectivity (i.e. target specific synapses rather than specific neurons). Our strategy to achieve this goal builds on the use of non-mammalian transplants to create a synthetic synapse. The mode of modulation comes from pre-synaptic uptake of a synthetic neurotransmitter (SN) into synaptic vesicles by means of a genetically targeted transporter selective for the SN. Upon natural vesicular release, exposure of the SN to the synaptic cleft will modify the post-synaptic potential through an orthogonal ligand gated ion channel. To achieve this goal we have functionally characterized a mixed cationic methionine-gated ion channel from *Arabidopsis thaliana*, designed a method to functionally characterize a synthetic transporter in isolated synaptic vesicles without the need for transgenic animals, identified and extracted multiple prokaryotic uptake systems that are substrate specific for methionine (Met), and established a primary/cell line co-culture system that would allow future combinatorial testing of this orthogonal transmitter-transporter-channel trifecta.

Synthetic synapses will provide a unique opportunity to manipulate synaptic communication while maintaining the electrophysiological integrity of the pre-synaptic cell. In this way, information may be preserved that was generated in upstream circuits and that could be essential for concerted function and information processing.

Acknowledgments and Dedication

“Success is not final, failure in not fatal; it is the courage to continue that matters”

- unknown author

The above quote is one that I feel defines the scientific spirit, but more than that it is what I believe defines excellent scientists and mostly for me, embodies the greatest lesson I learned from Dr. Harald Janovjak who, whether through observation and sometimes more direct means, taught me this over the years. I would like to thank Harald for his tireless support of my good ideas and his guidance out of the bad ones. I would like to thank him for allowing me to apply creativity and imagination to that which deeply interested me and for listening patiently to ALL my ideas. Things I have found to be a rare commodity from the head of scientific lab. His door was always open and no matter how big or small the issue was he found time to redirect his attention to help me - or at least give me the “I know you can figure this out” look, which was usually sufficient. Due to all of this and much much more, I have found a clear vision for my scientific career, which even now, at the end, when it is his right to bale as fast as possible – still offers me that which he did the first day in his lab, his opinion and his guidance without charge, so to say. I learned many things in my time in the Janovjak lab; that organization is the key to a happy life (still in the mist of learning this one), understand when to listen and when to plan secret projects, that sleep and diet are in fact extremely important to productivity, but by far the most memorable came many times over the years, from the inside of the office next to me, in a progress report, when I was so frustrated it was dangerous to be within arms-length of me, and that lesson is this - it’s all going to be OK – and frankly, in the end, it was. So for the times when I was right about the literature or a hunch or an experiment went as I planned, thanks Springsteen, for letting me take credit. I started my PhD thinking I could be a good scientist but being part of the Janovjak lab made me a good scientist.

I would also like to acknowledge Dr. Peter Jonas for the opportunity to join the IST graduate program and for his generousity for granting me use of lab space and resources. I would like to deeply thank all members of the Jonas group who were a constant for me with their tireless support in all things electrophysiological. Over my

years at IST there were many others that gave me so much of their time, knowledge, and assistance – but the two that must be mentioned by name are Yoav Ben-Simon, who always (and I mean always) had time to discuss experiments and in the end was instrumental in obtaining the final piece of post-synaptic proof of concept that I had work so tirelessly to realize, and Alexander Johnson for his superman abilities in all things imaging.

I would also like to acknowledge the other mentors in my life – for which without them I would never have made it to this stage. To Dr. James Rohr, who gave me the coolest opportunities of my professional life - flight simulation in the Cobra helicopter at Miramar, clearance onto the Navy SEAL base in Coronado, entry to the secret aquarium at Scripps Institute of Oceanography, the opportunity to design and implement my own scientific outreach program at Chompers Middle School - to name but a few. It was during this time that I found my passion for neuroscience and I am not convinced that would have happened without James' mentorship and guidance. James believed in my scientific abilities at moments when I didn't and whose smile and laughter was contagious. You were my mentor and my friend and I will miss you always. To my parents, Christine and Sean, there are simply no words to describe everything that you both have given me throughout my life and so I will simply say, this is yours as much as it is mine and I dedicate it to you.

Finally, to Bear, for all the late night dinners and for being the only reason I ate vegetables, for the countless words of love and encouragement, for your patience and understanding of my passion and dedication to this work and as a consequence, the late nights, the every weekend, the no vacations, the exhaustion…but mostly for all the love and laughter and Mexican food, for orange groves, for CDLB84E, for everything – thank you.

About the Author

Catherine McKenzie completed her BSc in General Biology with an emphasis on Neuroscience at the University of California, San Diego in combination with internships at the Space and Naval Warfare Systems Outreach Division (SPAWAR) at the US Department of Defense and Scripps Institute of Oceanography as well as implementing science education outreach programs in San Diego before joining IST in September 2011. Her main research interests lie in approaching old problems in new ways by designing and building biological methods to specifically address how tangible elements of the mammalian brain translate to cognitive processes and behavioral output. During her PhD studies she has published a springer book chapter on methodology of implementing light-gated ion channels in neuroscience research. As well as being a part of the IST doctoral program, Catherine was accepted as an Associate PhD student in the Molecular Drug Targets doctorate program funded by the Austrian Science Fund in Vienna, Austria in 2015. She was awarded the golden sponge for outstanding Teacher's Assistant in 2014 at IST. She has presented her work at a range of scientific platforms including the Casual Neuroscience FENS-IBRO Summer School in Bertinoro, Italy in 2013, the Gordon Research Seminar and Conference in Synaptic Transmission in the United States in 2016 as well as at the Society for Neuroscience conference in the United States in 2017. She was an invited speaker at the March for Science in Vienna 2017 and gave a Young Scientist Invited talk at the Joint meeting of Austrian Neuroscience Excellence Network in Alpbach, Austria in 2018.

Table of Contents

List of Figures

List of Tables

List of Abbreviations

AMPAR, α-amino-3-hydroxy-5-methyl-4-isoxazolepropionic acid receptors

Arg, L-arginine

AtGLRs, *Arabidopsis thaliana* glutamate-like receptors

BBB, blood brain barrier

BCH, 2-aminobicyclo[2.2.1]heptane-2-carboxylic acid

BSA, bovine serum albumin

BW, band width

CGC, cerebellar granule cell

CMV, human cytomegalovirus

CNS, central nervous system

DG, dentate gyrus

DIV, day *in vitro*

Dopa, dopamine

ECS, extracellular solution

EDTA,

ER, endoplasmic reticulum

ESS, extra-synaptic solution

FBS, fetal bovine serum;

ɣ2, stargazin

GABA, ɣ-aminobutyric acid

GLRs, plant glutamate-like receptors

Glu, L-glutamate

GluN1, glutamate ionotropic receptor NMDA type subunit 1

GPCRs, g-protein coupled receptors

HEK , human embryonic kidney

HNC, hippocampal neuronal culture

hPGK, human phosphoglycerate kinase

HRP, horseradish peroxidase

hSyn, human synapsin

iGluRs, ionotropic glutamate receptors

ISF, interstitial fluid

Kir1.2, inwardly rectifying voltage-gated potassium channel 1.2

LAT1, L-type amino acid transporter type 1
LBD, ligand binding domain
LGIC, ligand gated ion channels
MAP2, microtubule associated protein 2
Met, L-methionine
NMDAR, N-methyl-D-aspartate receptor
NT, neurotransmitter
PBS, phosphate buffered saline
PCR, polymerase Chain Reaction
PDS-95, post-synaptic density protein 95
PEI, polyethylenimine
PFA, paraformaldehyde
PI, preincubation
PLL, poly-*L*-lysine
PLO, poly-*L*-ornithine
PM, plasma membrane
RT, room temperature
SNAT2, ɣɣsodium-coupled neutral amino acid transporter type 2
SP, signal peptide
STED, stimulated emission depletion
SV, synaptic vesicle
Syp, synaptophysin
TARP, transmembrane accessory protein
TCA, trichloroacetic acid
TIRF, total internal reflection fluorescence
VGluT1, vesicular glutamate transporter 1
VM, vesicular membrane
WB, western blot
βnAchR, neuronal nicotinic acetylcholine receptor β subunit

Introduction

The mammalian central nervous system is one of the most complex maps on which information flow exists, even if compared to the Internet, which is the largest computer network established to date and currently consists of close to two billion websites [1]. In comparison, the number of neurons in canonical mammalian model systems used in research ranges from ~30 million (in mice) to ~100 billion (in humans) [2] with each neuron making upwards of a thousand synaptic connections [3]. This degree of complexity at the single neuron level translated en masse reveals a connectivity map with trillions of nodes.

The analysis of neuronal connections and their role in a specific animal behavior has been one of the defining aspects in our understanding of higher cognitive functions for more than a century [4] and yet today researchers are still disentangling neuronal connectivity, both morphologically and functionally. The ebb and flow of information transfer in the mammalian brain is sometimes paraphrased as a repeated analog-to-digital conversion [5, 6]. This conversion, which has been observed in the visual system, the hippocampus and neocortex of rodents [7-9], is one of the hallmarks of complexity in the mammalian brain and a result of the interplay of multi-tiered regulatory elements, such as gene activation or suppression, protein regulation and activation, signaling cascades, and cell-cell type interactions [10-15]. A macroscopic example of this conversion is the concept of convergence, in which many pre-synaptic digital outputs translate to many post-synaptic analog inputs, all of which are computed to a singular digital output (firing or no firing) of the post-synaptic cell [16]. It is the combination of multiple inputs in time and space that allows information to be passed on in a manner that is modulated by upstream regulation. The breakdown of this computation process can have devastating effects, and often because of its fundamental role in physiology results in neurological diseases, such as motor dysfunction (e.g. Parkinson's [17, 18], Huntington's [19-22], disease), inhibitory dysfunction (e.g. autism spectrum disorder [23]), and memory loss (e.g. Alzheimer's disease [24-26]).

To understand the significance of activity in individual connections mapping of inputs and outputs in the intact tissue is a prerequisite. Great strides have been made through the use of advanced genetic strategies including Brainbow [27, 28], imaging,

high throughput EM [29], and viral tracers [30, 31] to understand cell type connectivity within and across brain regions. Yet, our understanding of the functional relevance of the mammalian brain connectome is far from complete [32] and there is an ongoing need for new methods to allow finer functional control over morphologically defined connections.

The introduction of exogenous electrical signals into excitable cells, either electrically (e.g. using electrodes) or remotely (as explained below) is a powerful form of manipulation towards elucidating determinates of information flow in the nervous system and has historically been the method of choice. Many modern implementations incorporate biological tools in intact circuits *via* genetic perturbation that have been designed to exert control over defined cellular populations. The move from *in vitro* studies to the intact organ in behaving animals posed new challenges in the application of these techniques, such as the difficulty to alter neuronal behavior in a targeted fashion. These challenges have been successfully met with the genetic introduction of various tools, most notably, optogenetics [33, 34] and chemogenetics [35, 36]. However, the current toolbox that allows for a causal relationship between cell type and behavior employs a brute force induction that is often binary. Thus new methodology that reflects the non-linearity of information flow by mimicking analog-like responses may become an important new approach to our understanding of brain function in health and disease.

This work focused on the design of new biological tools and methods that will help to dissect neuronal connections and their impact on organism behavior by targeting the neuronal analog-to-digital conversion. This goal was achieved by hypothesizing a synthetic neurotransmission (SNT) system that preserves upstream information while simultaneously manipulating the computation of the post-synaptic target (chapter 1), characterizing a methionine-gated cation channel as a candidate for the SNT receptor (chapter 2), permeable to Ca^{2+} as a chemogenetic tool that can be tuned for graded bioelectrical responses in mammalian cells, and developing a new method to understand the relationship of proteins involved in pre-synaptic release in chemical transmission by altering protein content in isolated synaptic vesicles *in vitro* (chapter 3). This work furthermore addresses future experimental designs to test the pre-synaptic incorporation for a synaptically selective post-synaptic override method (chapter 4).

Chapter 1: Synthetic Neurotransmission: Manipulating Neuronal Communication with Intrinsic Encoding and Connectivity

This chapter is a hypothesis manuscript in preparation (Catherine McKenzie and Harald Janovjak, 2018).

1.1. Abstract

A major challenge in neuroscience research is to dissect the circuits that orchestrate behavior in health and disease. Here, we hypothesize that this challenge may be tackled by extending current concepts and existing methodologies with a synthetic neurotransmission (SNT) system. Specifically, we propose a synthetic neurotransmitter that will be taken up and loaded into pre-synaptic vesicles that have been genetically-modified with new and orthogonal membrane transporters. Upon vesicle release triggered by the natural firing pattern of the neuron, the synthetic neurotransmitter will activate specific post-synaptic neurons that synaptically express a new and orthogonal receptor. Because of the necessity of introduced transporters and receptor, SNT will allow targeting of selected synapses in a circuit and in addition exploit endogenous firing patterns for modulation of neuronal activity. This approach is thus complementary to light-activated ion channels and orthogonal ligand-receptor-pairs, which target selected neurons and override their natural activity patterns. In this hypothesis article, we describe the motivation for developing SNT, explain the possible strategies to experimentally realize it and speculate how SNT will open new research avenues for decoding neural circuits, understanding of the intricacies of synaptic communication and developing disease models

1.2. Hypothesis

The development and function of all multicellular organisms relies on ordered communication of cells. The nervous system offers a prime example for the importance of ordered cell-cell communication that has been extensively investigated throughout the last three centuries. The concept of synapses (Greek: synapsis - junction) emerged at the end of the nineteenth century when Santiago Ramón y Cajal predicted synapses as “contacts at the level of certain apparatus or dispositions of mechanisms, whose objective is to establish connection” [37]. The term ‘synapse‘ was coined by Charles Scott Sherrington in 1897 at a time where the prevailing theory for interneuronal communication was based on electrical signals [38]. Two ground breaking hypotheses, the chemical nature of communication and the existence of specific receptors for chemical agents, revolutionized our view of neuronal communication at the turn of the century [39, 40]. With the advent of chemical

synthesis, genetics and molecular biology, the twentieth century led to the identification and characterization of components fundamental in synaptic communication. Acetylcholine was the first chemical neurotransmitter to be synthesized, and it was shown to activate cells about sixty years before the genetic identity of acetylcholine receptors was revealed [41-43]. The discovery of acetylcholine was followed by the discovery of GABA, serotonin, glutamate, dopamine and glycine within the 1950s and 60s [44-48]. While the components driving many aspects of neuronal communication have been demystified in the past two centuries, one on-going challenge in this century is to discover how they orchestrate activity in health and disease. Here, we hypothesize that we may tackle this challenge by extending current concepts and existing methodologies with a synthetic neurotransmission (SNT) system that operates orthogonally to normal neuronal communication.

Relaying the correct information from one area of the nervous system to another requires synapses working *en masse*. In the typical mode of synaptic communication, electrical spiking in the axon of the pre-synaptic neuron results in neurotransmitter release from pre-synaptic vesicles and activation of receptors on the post-synaptic cell (Fig 1.1A). Disruption of connectivity leads to serious behavioral malfunctions observed in neurological diseases, which has had the positive side effect that scientists were inspired to create new methods to enhance or reduce neuronal activity. The birth of many recent methods to manipulate neurons coincided with the emergence of synthetic biology in the neurosciences. Highlights of synthetic biology contributions are the repurposing of naturally-occurring opsins [33], such as channelrhodopsin from *C. rheinhardtii*, and the engineering of semi-chemical systems [49], for the optical actuation or inhibition of neuronal firing. The light-sensitive proteins are complemented by ‘orthogonal’ receptors designed to be sensitive to non-natural ligands [50-52] (Fig 1.1B), each of which are masterpieces of protein engineering. Paired with advancement in genetic targeting to selected neuronal populations, these methods allowed scientists to gain unparalleled access to the inner workings of the nervous system in many model organisms. In particular, optical manipulation of genetically-selected neurons with high spatial (micrometers to centimeters) and temporal (milliseconds to minutes) has allowed deciphering the necessity of subtype specific signals, i.e. interneurons, and delving into behavior linked to specific neurons within a circuit.

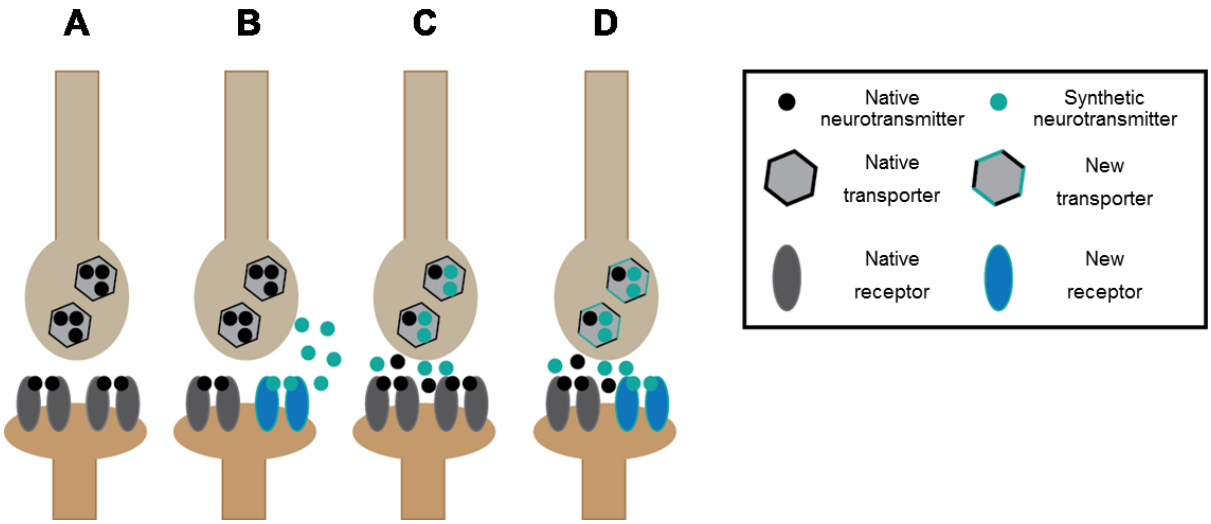

Fig 1.1. Modulating a synapse with a synthetic neurotransmitter Comparison of (A) native synaptic transmission, (B) orthogonal receptor-ligand-pairs [50-52], (C) false neurotransmitters [53, 54], and (D) SNT that is proposed here. The synthetic neurotransmitter is only taken up by cells that express new transporters. Also, the synthetic neurotransmitter selectively activates cells that express a new ligand-gated ion channel. Thus only selected synapses are modulated by SNT .

Currently it is not feasible to manipulate neuronal communication in a manner that closely incorporates the functional intricacies of synapses. For instance, activation or inhibition by light and orthogonal ligands imposes firing patterns and selects synapses in manner that is limited by the fidelity of spatially-confined illumination or diffusion. To complement the existing methodological arsenal, we propose to develop methods that on one hand allow experimenters to intervene with neuronal connections from the outside, as with the tools described above, while preserving encoding and connectivity. Specifically, we hypothesize that this may be achieved by creating a synthetic neurotransmitter, which we define as a non-native small molecule that produces additional post-synaptic responses upon pre-synaptic vesicular release. The synthetic neurotransmitter could be added to systems in vitro or *in vivo*, e.g. by systemic injection, at the time that manipulation is desired, yet would exclusively

function at selected synapses between cells that were ‘sensitized’ (Fig 1.1D). Sensitization of the pre-synaptic cell will be achieved by expression of transporters engineered for uptake and release of the synthetic neurotransmitter. Sensitization of the post-synaptic cell will be achieved by expression of an ionotropic receptor engineered to be selectively activated by the synthetic neurotransmitter. Because synthetic neurotransmitters act as neurotransmitters only at synapses between cells that were genetically-modified they may enable many new types of experiments (see below). This idea extends the concept of ‘false neurotransmitters’, which also are non-natural small molecules packaged into synaptic vesicles (Fig 1.1C) but serve to visualize vesicle fusion or activate selected endogenous post-synaptic targets [53, 54]. Already in 1993, Jahr and co-workers demonstrated the principle of false neurotransmitter signaling at glutamatergic synapses (Pan et al, 1993), but very few studies followed up on this clever approach, with one elegant example being the false fluorescent neurotransmitters at dopamine synapses [54].

Which new experiments will be enabled by SNT? First, SNT may aid in deciphering of neural circuits. The technique will impart the ability to modulate specific neural connections because it effectively targets synapses rather than neurons. In principle, all synapses of a connection may be targeted because modulation is generated intrinsically and may be applicable also in those cases where selection of projections by confined illumination is not possible. Second, synthetic neurotransmission may shed new light on the many fundamental processes that are controlled by temporal activity and vesicular release patterns, such as synaptic plasticity or dendritic integration. New experiments will be enabled because the technique will preserve firing patterns in the pre-synaptic cell and modulate the post-synaptic signal in strength based on this intrinsic pattern. In this way information may be preserved that was generated in upstream circuits and that could be essential for concerted function and information processing. In complementary experiments, it should also be possible to introduce the ligand-gated ion channel into pre-synaptic cells and use the synthetic neurotransmitter as a retrograde messenger. Third, taking advantage of the preservation of temporal firing patterns, SNT may lead to the development of models of disease and drug action, because in both cases gradual modulation of synaptic communication is imparted.

We have entertained three paths to realizing SNT in the mammalian nervous system. First, mammalian ligand-gated ion channels and neurotransmitter transporters may be reengineered through mutagenesis to interact with a molecule that is otherwise inert for the neuronal signaling machinery. This molecule may then, preferably after passing the blood brain barrier, act as the synthetic neurotransmitter between cells modified with the engineered ligand-gated ion channel and transporters. Indeed, altering binding specificity of receptors through mutagenesis was successful in the past for ligand-gated ion channels and G-protein coupled receptors [50-52]. However, the encouragement that this past work provides is mild because the chemical and genetic space that needs to be sampled during engineering is substantial and because less precedence exists for engineering of membrane transporters. Second, an entire mammalian neurotransmission machinery, consisting of the neurotransmitter, ligand-gated ion channel and transporters, may be introduced into brain regions where it normally is not found. Although this appears to be a straightforward approach our analysis of the mouse brain suggest that likely all major brain regions are innervated by most if not all neurotransmitters, which reflects that the nervous system is efficient at employing a relatively short list of messenger molecules. This approach thus may be limited in terms of orthogonality, flexibility and reliability. Third, a set of non-mammalian proteins, including ligand-gated ion channel and transporters, may be transferred to the mammalian brain. In this way the design of matching binding sites can be ‘outsourced’ to Nature based on the hypothesis that the diverse habitats of various species have produced proteins responsive to ligands not found or not used in the mammalian nervous system [55, 56]. This approach removes the need for binding site engineering but requires that a ligand-gated ion channel and transporters for the same molecule can be identified and expressed functionally in mammalian neurons. Interestingly, the light-driven proton pump Arch was recently targeted into neuron vesicles [57], and this work demonstrates that mammalian vesicles can be ‘functionalized’ with a non-mammalian membrane protein. Finally, a combination of the second and third approach may be envisioned, e.g. based on dopamine-gated ion channels [58]. Notably, all three approaches discussed above benefit from many of the techniques that already enabled the success of synthetic neurobiology, such as viral vectors, Cre-dependent expression or *de novo* synthesis of mammalian codon-optimized genes.

To summarize, we conclude that SNT may become a valuable asset for the understanding of nervous system function on several levels ranging from microcircuits to *in vivo* behavior and that its technical realization may be may be possible, an effort we believe is worth pursuing.

Chapter 2: Repurposing a Methionine-gated Ionotropic Receptor for Orthogonal Control of Bioelectrical Activity in Mammalian Cells

I would like to thank Marco Stadler (Department of Pharmacology and Toxicology, University of Vienna) who performed all oocyte experiments and Daniel Tapken (Ruhr University Bochum) for the AtGLR1.4 pore point mutation as well as numerous insights into AtGLRs. I would also like to thank Giulio Abagnale for his assistance with STED imaging, Ben Suter and Alexander Johnson for their insights on image analysis, and Yoav Ben-Simon who performed viral injections, subsequent perfusion, slice, and mounting. In addition I would like to thank Dr. Ryuichi Shigemoto for the custom GluA2 antibody. This chapter is a research manuscript in preparation (Catherine McKenzie, Daniel Tapken, Marco Stadler, Yoav Ben-Simon, Giulio Abagnale, and Harald Janovjak).

2.1. Abstract

Understanding the significance of cellular and subcellular communication between and among neuronal circuits is a fundamental goal in bridging the gap between the tangible elements of the brain and behavior of an organism. The biological toolbox that has been developed to override communication has in recent years incorporated genetically targeted designer receptor-ligand pairs referred to as chemogenetics, which allows specified modulation of cell-type specific behavior upon activation of a synthetically derived ligand. Here we have identified and expressed a modified plant glutamate-like receptor, iMetR in HEK 293 cells and neurons as a way to modulate bioelectric activity in mammalian cells by making use of its evolutionarily derived "designer" ligand, methionine and calcium permeable mixed cationic pore conducting properties. Taking advantage of its analogous secondary structure to ionotropic glutamate receptors we were able to target variants of iMetR subcellularly and show that methionine application in mammalian cells that express iMetR or variants induce bioelectric signals in a synthetic manner.

2.2. Introduction

Decoding the roles of specific neuronal and non-neuronal cell types in complex behaviors and physiological processes is fundamental to our understanding of brain function in health and disease. 'Synthetic' perturbation of electrical signals by means of introduced receptors and ion channels has proven to be an invaluable approach to examine the link between cellular activity and organism function. The current toolbox consists of designer receptors that are classified by their cognate actuators, which are either photons (in optogenetics) or chemicals (in chemogenetics). Specifically, optogenetic and chemogenetic receptors engineered to respond to light or highly selective 'designer' molecules have enabled researchers to resolve the key determinates that underlie observable behaviors *in vivo*, such as taste differentiation, hunger and pleasure states, as well as memory encoding [33, 59-62]. Ion channels are particularly well suited for this purpose because they create additional ion fluxes that augment or override native physiological electrical activity states. The channels can be selected or engineered for characteristic depolarizing or hyperpolarizing

conductances [63, 64] to ultimately direct cell behavior in defined spatial and temporal locations.

Chemogenetic tools for neuronal manipulation have in the past been based on ligand-gated ion channels (LGICs) [50, 64] and G-protein coupled receptors (GPCRs) [51, 52, 65, 66]. In their most advanced form, these proteins are synthetically altered to attenuate native ligand reactivity while exhibiting sensitivity to a novel ligand. All of the current tools rely on redesign of a native protein in conjunction with the use of a synthetic agonist [50, 52, 64]. Whereas these designs have been successful they can be accompanied by limitations, such as lack of blood brain barrier (BBB) permeability [67], incomplete orthogonality [64], reliance on second messenger pathways [51, 52], need for heteromeric subunit assembly [64], and potentially unsought interactions with endogenous proteins. A desirable alternative to synthetic orthogonality would be to take advantage of the evolutionary lineage of LGICs. Identifying homologs that retain neuronal modulation properties, such as the desired ionic selectivity, yet disclude orthogonality issues, such as activation by native molecules, may be a complementary and potent alternative. Here, we hypothesized that plant glutamate-like receptors (GLRs) carry many of the attributes of an ideal receptor-ligand pair.

Ionotropic GluRs (iGluRs) are specialized mammalian GLRs that are irreversibly intertwined in the computation of cells involved in cognitive processes like learning and memory, as well as homeostatic regulation/innate physiology [68]. iGluRs are mixed cation permeable (of physiological relevance are Na^+ and K^+ and finely tuned additional Ca^{+2} permeabilities) and cluster post-synaptic loci to mediate excitatory ionic conductance. Due to the nature of iGluRs and their pivotal roles in electrical-activity driven systems, the discovery of GLRs in plants (e.g., AtGLRs in the important model plant *A. thaliana*) was unforeseen but fortuitous. AtGLRs have similar ionic preferences to iGluRs [69-71] that makes them potential candidates for chemogenetic tools if orthogonality in ligand binding is intrinsic or can be introduced.

The family of AtGLRs diverges into three clades exhibiting conserved structural topology with the mammalian glutamate receptors (GluRs) [63, 72]. AtGLR1.4, a member of clade 1, has been well-characterized in both structure and function [63]. Notably, the ligand binding domain of AtGLR1.4 has no potency for glutamate or many of the major neurotransmitters in the mammalian central nervous system (CNS) [63], but rather is a methionine-gated, Ca^{+2} permeable mixed cation channel [63]. Met is an

essential amino acid that plays multiple key roles in mammalian metabolism but does not activate mammalian receptor proteins. Prior uses in humans as a dietary supplement, as an antidote or in CNS cancer imaging indicate a safe and well known pharmacological profile making it suitable as a designer ligand.

Here, we show that an optimized variant of AtGLR1.4, termed iMetR, expresses well in a number of expression systems and neurons, both *ex* and *in vivo*. This channel shows detectable current when its agonist Met is applied and can be blocked by its natural antagonist arginine (Arg). Combined, this translates to a chemogenetic "on/off" switch for bioelectric activity in mammalian cells. In addition, ligand profiling revealed the ability to remotely switch activation states in a graded fashion, by tuning Met concentrations in a simulated *in vivo* environment. In this chapter, we present the first example of the functional expression of a clade 1 plant glutamate-like receptor in mammalian cells, paving the way for future repurposing for neuronal modulation. As outlined in chapter 4, endogenous and exogenous Met transport systems exist and AtGLR1.4 may be combined with those to achieve synthetic neurotransmission (SNT) relying on its graded response to Met in antagonistic-containing buffers.

2.3. Methods

2.2.1. Animals

All animal experiments were performed in strict accordance with institutional, national, and European guidelines for animal experimentation and were approved by the Bundesministerium für Wissenschaft, Forschung und Wirtschaft of Austria (A. Haslinger, Vienna; BMWFW-66.018/0007-WF/II/3b/2014)

8 week old C57BL/6J mice were put under light anesthesia via isoflurane and placed into a head fixed stereotaxic frame (RWD Life Science). Animals were kept under anesthesia with a continuous flow of 1-3% vaporized isoflurane, mixed with 100% O_2 at a flow rate of 0.5 L/min. Incision was made front to back to expose the skull and the bregma was located. Two small holes were drilled above the dorsal dentate gyrus (DG) bilaterally and the durum was gently removed. 0.5 µL concentrated lenti virus (see below) was injected bilaterally at a rate of 100 nL/min using a syringe (Hamilton) fixed with a 33G needle into the dorsal DG at coordinates ±1.5 mm medial/lateral, 1.8 mm anterior/posterior, 1.9 mm dorsal/ventral from the bregma. Animals were kept in

their home cage with ad lib water and food for 2 weeks. Mice were perfused with 15 mL phosphate buffer (0.1M Na_2HPO_4 and 0.1M NaH_2PO_4 titrated to pH 7.35) followed by 15 mL 4% paraformaldehyde (PFA). Fixed brains were sectioned coronally at a thickness of 100 µm using a Leica VT1200S vibratome. Slices were mounted on micro slides (Assistant) with Mowiol mounting media (6 g glycerol, 2.4 g Mowiol® 4-88, 12 mL 0.2 M Tris-HCl) and covered by 0.15 mm glass coverslips.

2.2.2 DNA constructs

pSGEM::AtGLR1.4, pSGEM::AtGLR1.4(C610W), and pSGEM::GluA2(Q)flop(L483Y) vectors were a generous gift from Daniel Tapken(RUHR University BOCHUM). Stargazin (γ2) vector was a generous gift from Daniel Choquet (University of Bordeaux). GluA2(flop)_eGFP was a generous gift from Maximilian Ulbrich (University Freiburg) and mVenus was a generous gift from Richard Tsien (New York University). iMetR1.0, a variant of AtGLR1.4 (Uniprot-ID Q8LGN1) was modified for mammalian expression, adapted from previous work on iGluRs and opsins [49, 73]. Applying conventional cloning strategies, AtGLR1.4 was extracted from pSGEM::AtGLR1.4_eYFP by Polymerase Chain Reaction (PCR) and subcloned into a modified mammalian expression vector driven by the human cytomegalovirus (CMV) promoter (pcDNA3.1(-), Invitrogen/Life Technologies). The modified vector contained a membrane trafficking signal (VNIKSRITSEGEYIPLDQID, Addgene 26966), eYFP (Addgene 26966), and ER export signal (KFCYENEV, Addgene 26966) for enhanced receptor trafficking and membrane expression followed by a WPR element [49] after the stop codon. In the resulting construct, the AtGLR1.4 signal peptide (SP) (amino acids 1-29) was exchanged for the neuronal nicotinic acetylcholine receptor β subunit (βnAchR) SP (amino acids 1-18, GenBank: CAA33839.1, [74]. A mutation from cysteine (C) to tryptophan (W) in AtGLR1.4 at position 610 (, designed to increase channel conductance, was identified by Daniel Tapken (Hollmann lab, RUHR University BOCHUM) and was introduced into iMetR1.0 at position 599 as well as mutations to Alanine, Serine, or Tyrosine through site-directed mutagenesis [75]. iMetR1.0ΔC599W was mammalian codon optimized according to the supplier's recommendation (Epoch Life Sciences) with an additional AgeI site introduced at position (874-5) directly after the Kv1.2 membrane trafficking signal. An mVenus amplified by PCR and inserted into the Age1 site and the resulting construct renamed

iMetR. C-terminal variants iMetRΔR2ct and iMetRγ2$_{15}$ were designed by introducing an AgeI (iMetRγ2$_{15}$), or replacing the entire AtGLR1.4 C-terminus (CT) (iMetRΔR2ct, 811-850) with an AgeI restriction site at position 850 (YLIPW**TG**KSRITS) into iMetR using reverse PCR. A synthesized cDNA fragment (Integrated DNA Technologies) corresponding to the CT of GluA2 (R2) (UniProtKB: P19491 GR1A2_RAT) or 5'phosphorylated ultramers (Integrated DNA Technologies) encoding the PDZ-binding motif of Stargazin (ɣ2$_{15}$) (UniProtKB: 088602 CCG2-MOUSE) were subsequently subcloned into pcDNA3.1(-)::CMV::iMetR in corresponding places (see above). pCCL viral vectors (9765382) containing iMetR, iMetRΔR2ct, and iMetRγ2$_{15}$ between NheI and SalI were modified for targeted neuronal expression by swapping a human phosphoglycerate kinase (hPGK) promoter for a human synapsin (hSyn) promoter. GluA2(flop)_eGFP, AtGLR1.4_eYFP, iMetR and all variants were expressed either under the control of CMV promoter for cell line expression or the hSyn promoter for neuronal expression. All constructs were verified in frame by sanger sequencing (LGC genomics).

2.2.3. HEK 293 cell culture

For whole cell patch clamp and imaging, HEK 293 cells were seeded in D5 (Dulbecco's modified Eagle's medium (Life Technologies) supplemented with 5% v/v fetal bovine serum (FBS, Life Technologies), at a density of 3.0-8.0 x 10^4 on poly-*L*-lysine (PLL) coated 12 mm glass coverslips as described previously [76]. Briefly, coverslips (A. Hartenstein, 0.17 mm) were prepared by washing once with 100% ethanol followed by 5 washes with ultrapure water (Life Technologies). Coverslips were further autoclaved and dried in an oven (HEREAUS, 120°C for 2h) followed by UV sterilization. Coverslips were coated for 1-2 h before plating with PLL (0.1% w/v, Sigma in water) washed once with ultrapure water and allowed to dry completely. For imaging, 24-well glass bottom plates were treated as above with the exception of autoclaving. Cells were transfected at equal molar ratios with lipofectamine 2000 (1mg/mL, Life Technologies) at a 1:1 (µg/µl) ratio where applicable, in Opti-MEM I medium (Gibco) 18 h after seeding. Medium was changed to D5 (electrophysiology) or D10 (Dulbecco's modified Eagle's medium (Life Technologies) supplemented with 10% v/v FBS, 100 U/ml penicillin and 0.1 mg/ml streptomycin) (imaging) after 7 h and incubated at 37°C in a 5% CO_2 atmosphere for 48-72 h. For imaging, 24 h after transfection cells were transferred to

33°C in a 5% CO_2 atmosphere and incubated for another 24-36 h [77]. Cells were imaged either in modified tyrode solution (TIRF) (NaCl 150 mM, KCl mM, $MgCl_2$ 2 mM, $CaCl_2$ 2 mM, D-Glucose 10 mM, HEPES 10 mM pH.4) or fixed with 4% PFA (confocal) and maintained at 4°C in PBS 0 - 2 d before imaging.

2.2.4. Lenti virus production

Lenti virus production and purification was performed as described previously [78]. 7.0 x 10^6 Lenti-X 293T cells (Clontech) were seeded in D10 in poly-*L*-ornithine (PLO) (0.01% w/v, Sigma) coated 15 cm cell culture dishes (Corning) and incubated at 37°C in a 5% CO_2 atmosphere. After 15 h, medium was changed and cells were incubated at 37°C for 30 min. Cells were then transfected with pccl::hysn:: iMetR or variants of MDL and REV (third generation pHelper plasmids), and VSV-G (packaging plasmid) at a 1:1:1:1 molecular ratio (total amount: 28 µg per dish) with polyethylenimine (PEI) (Polysciences) in Opti-MEM I medium. Medium was changed 7 h after transfection. 40-48 h after transfection, supernatant was collected for centrifugation at 1,000 x g for 10 min, and subsequently filtered (0.45 µm). For virus concentration, filtered supernatant was layered over a 10% v/v sucrose cushion (20% w/v sucrose in 1 M NaCl, 20 mM HEPES, 0.25 mM EDTA, pH 7.4) and centrifuged at 4°C for 1.5 h at 150,000 x g. During 2 to 4 separate centrifugation runs, pellets were consolidated and resuspended in culture medium (see below) and stored at 4°C. After centrifugation, concentrated virus was either aliquoted directly or further concentrated with Vivaspin® centrifugal concentrator (Vivaproducts) for *in vivo* applications. Virus was aliquoted into O-ring conical tubes, snap frozen and stored at -80°C. Physical titer was determined using a reverse transcriptase qPCR kit following the provider's protocol (Genecopia). Each viral preparation was tested for functional expression with a dilution series in glass bottom 24-well plates containing 2.5 x 10^5 cortical neurons/well. After 5 d, expression was assessed daily using an EVOS FL microscope (Thermo Fisher Scientific). The virus concentration that produced the highest expression in morphologically healthy cells at day *in vitro* (DIV) 15 was then utilized for transduction of neurons on 12 mm glass coverslips (see below). For *in vivo* injections titers of between 1 x 10^9 - 10^{11} viral particles/mL were used.

2.2.5. Primary neuronal culture

Primary dissociated hippocampal neurons were prepared from batches of 2-4 P0-P1 Wistar rat pups as described previously [76] with modifications as follows. Hippocampi were isolated from both hemispheres in dissecting solution (Hank's balanced salt solution supplemented with 2.5 mM HEPES, 35 mM D-glucose, 4 mM $NaHCO_3$, pH 7.4) by removing midbrain, cerebellum and olfactory bulb and clearing the meninges from the tissue. Cortical hemispheres were flipped sagittally and hippocampi were removed with fine tip forceps and transferred to a 15 mL conical tube filled with dissecting solution on ice. Dissociation was carried out using a papain dissociation system following the provider's protocol (Worthington). Neurons were maintained following established protocols [79] with modifications. Cells were suspended in plating medium that consisted of modified Eagle's medium (MEM) (Thermo Fisher Scientific) supplemented with 10% v/v FBS, 0.6% w/v D-glucose (Sigma), 6 mM GlutaMAX™ (Thermo Fisher Scientific), 1 mM Na-pyruvate (Sigma), 100 U/mL penicillin and 0.1 mg/mL streptomycin. Cells were counted in a Neubauer chamber and 0.5-1.0 x 10^5 cells were seeded on 12 mm glass coverslips (0.17 mm for electrophysiology or 0.15 mm for imaging) as prepared above. After 5 to 6 h, one volume of culture medium (Neurobasal-A (Thermo Fisher Scientific), supplemented with 2% v/v B27™ (Thermo Fisher Scientific), 6 mM GlutaMAX™) was added to each well. At DIV2 to DIV3, medium was supplemented with 4 µM cytosine β-*D*-arabinofuranoside (Sigma) to reduce glial growth. Finally, cells were transduced with lenti virus during medium change at DIV5 and subsequently half of the culture medium was changed every 2 to 3 d. Neurons were typically transduced with 0.1 µl of concentrated virus solution (1.0 x 10^9 viral particles/mL) and displayed robust expression at DIV15.

2.2.6. Electrophysiology

2.2.6.1. Xenopus laevis oocyte two-microelectrode voltage-clamp experiments

Preparation of stage V–VI oocytes from *Xenopus laevis* and synthesis of capped runoff poly(A) cRNA transcripts from linearized cDNA templates (pSGEM:: pSGEM::AtGlR1.4(C610W) and pSGEM::GluA2(Q)flop(L483)) was synthesized from 1 µg of linearized template DNA with the mMESSAGE mMACHINE T7 *in vitro*

Transcription Kit (Thermo Fisher Scientific). Preparation of stage V–VI oocytes from *Xenopus laevis* was performed as described elsewhere [80]. Female *Xenopus laevis* frogs were anesthetized by 15 min incubation in a 0.2% MS-222 solution (methane sulfonate salt of 3-aminobenzoic acid ethyl ester, Sigma) before removing parts of the ovaries. Follicle membranes from isolated oocytes were enzymatically digested with 2 mg/mL collagenase (Type 1A, Sigma). Selected oocytes were injected with 20–50 nL of DEPC-treated water (diethyl pyrocarbonate, Sigma) containing the different cRNAs at a concentration of 500 pg/nL/subunit. Oocytes were stored at +18°C in modified ND96 solution (90 mM NaCl, 1 mM $CaCl_2$, 1 mM KCl, 1 mM $MgCl_2 \cdot 6H_2O$, and 5 mM HEPES, Sigma). Recordings were performed at days 3-4 after oocyte injection. Currents through AtGLR1.4CΔ610W and GluA2(Q)flop(L483) receptors were measured at room temperature (20-24°C) by means of the two-microelectrode voltage clamp technique making use of a TURBO TEC-05X amplifier (NPI Electronic). Currents were elicited at a holding potential of -100 mV. Data acquisition was carried out by means of an Axon Digidata 1440A interface using pCLAMP v.11 (Molecular Devices). ND96 (96 mM NaCl, 1.8 mM $CaCl_2$, 2 mM KCl, 1 mM $MgCl_2 \cdot 6H_2O$, and 5 mM HEPES, Sigma) was used as bath solution. Microelectrodes were filled with 3 M KCl and had resistances between 1 and 3 MΩ.

2.2.6.2 Fast Perfusion System

Compounds were applied by means of a solution exchange system as described previously [81]; drug or control solutions were applied by means of a TECAN Miniprep 60 enabling automation of the experiments (ScreeningTool, NPI Electronic). To elicit currents, the chamber (holding volume 15 µL) was perfused with 250 µL of compound-containing solutions at a volume rate of 200 µL/s [82]. For experiments determining kinetic properties of the channel, solutions were applied at a volume rate of 400 µL/s. To account for possible slow recovery from increasing levels of desensitization in the presence of high compound concentrations, the duration of washout periods was extended stepwise, i.e. 1 min (≤3 µM compound) to 1.5 min (≤10 µM) to 2.5 min (≤100 µM) to 5 min (≤1 mM) to 15 min (≤10 mM). Oocytes with maximal current amplitudes >5 µA were discarded to exclude voltage-clamp errors. Concentration-response curves were generated, and the data were fitted by non-linear regression analysis using ORIGIN 7.0 (OriginLab Corporation). Data were fitted to the Hill equation: y =

min + (max – min) * xn/(k^{nH} + x^{nH}) with k corresponds to the EC_{50} value, x-values are logs of concentration, and nH is the Hill coefficient. Each data point represents the mean ± SEM from at least 2 oocyte batches. Data was analyzed in Clampfit 10.1. (Molecular Devices)

2.2.6.3. HEK 293 cells

Whole-cell patch-clamp recordings were performed as described [76] with modifications as follows. Pipettes (Bo-glass capillaries fire polished OD 2.0 ID 1.5 Hilgenberg) were pulled to resistances of 4-6 MΩ (Sutter Instruments) and were filled with an internal solution (135 mM K-gluconate, 6 mM NaCl, 4 mM MgCl2, 2 mM NaATP, 1 mM EGTA, 10 mM HEPES, pH 7.4). A home-made gravity perfusion system containing extracellular solution (ECS) (145 mM NaCl, 4 mM KCl, 1 mM $MgCl_2$, 2 mM $CaCl_2$, 10 mM HEPES, 10 mM sucrose, pH 7.4 adjusted with NaOH) alone or with 0.1 or 1 mM L- methionine or 1 mM L-arginine, was continuous at an average flow rate of around 40 - 80 µL/s. For amino acid profiling, ECS was exchanged for extra synaptic solution (ESS) ((0.14 mM L-arginine, 0.45 mM L-lysine, 0.025 mM L- valine, 0.005 mM L-cysteine, 0.05 mM L-threonine, 0.045 mM L-alanine, 0.05 L-histadine, 0.07 L-serine, 0.025 mM L-lysine, 0.015 mM L-isoleucine, 0.650 mM L-glutamine, 0.01 mM L-methionine in ECS, pH 7.4 all amino acids were added from fresh (<2 weeks at 4°C) 100-250 mM stock solutions made in house in H_20, Sigma)) and then exchanged for ESS containing 0.1 or 1 mM Met. Cells expressing AtGLR1.4_eYFP, iMetR or variants were identified using a polychrome V monochromator (Tillphotonics). Wavelength of 497 nm (bandwidth (BW) 16 nm, Thorlabs) was directed to either a 20, 40, or 63x objective (Olympus) using a Dichroic filter (R Band = 490–510 nm, T Band = 520–700 nm, Thorlabs) and an emission filter for 535 nm (BW 22 nm, Thorlabs) through an illumination port in the microscope (IX 50, Olympus). Data was acquired in voltage clamp mode with an Axopatch 200B amplifier (Axon instruments) controlled by pClamp 10 software with Digidata 1440A interface (Molecular Devices) 48-72 h after transfection and was recorded with pClamp 10 software (Molecular Devices), which was also used to regulate the polychrome. Data was filtered at 2 kHz. For current-voltage (I/V) relationships, current was first acquired in gap free mode at -70 and 0 mV

hold. Data was obtained using a ramp step protocol from -80 – +80 mV over 5 sweeps with a delay of 1 s between sweeps. Met I/V curves were plotted with a baseline ramp subtraction off line. All current analysis was performed offline in Clampfit 10.1 and further analyzed in Igor 6.34A (WaveMetrics).

2.2.6.4 Hippocampal Slice

Acute transverse hippocampal slices (400 µm thick) were prepared from mice 8–14 days post-injection (dpi). Briefly, the hippocampi were isolated and cut in a VT1000S or VT1200S vibrotome (Leica) in an extracellular solution containing 215 mM sucrose, 2.5 mM KCl, 20 mM glucose, 26 mM $NaHCO_3$, 1.6 mM NaH_2PO_4, 1 mM $CaCl_2$, 4 mM $MgCl_2$, and 4 mM $MgSO_4$. Thirty minutes after sectioning, the cutting medium was gradually switched to an artificial cerebrospinal (ACSF) recording solution containing 124 mM NaCl, 2.5 mM KCl, 26 mM $NaHCO_3$, 1 mM NaH_2PO_4, 2.5 mM $CaCl_2$, 1.3 mM $MgSO_4$, and 10 mM glucose. All solutions were equilibrated with 95% O_2 and 5% CO_2 (pH 7.4). Slices were incubated for at least 60 min in ASCF solution before recordings. Hippocampal slices were visualized using infrared differential interference contrast (IR/DIC) and GFP fluorescence. All slices included in this study exhibited strong fluorescence in dentate gyrus. Experiments were performed at 26.0°C ± 1.0°C in a submersion-type recording chamber perfused at ~1.5 ml/min with ASCF. Data was acquired in current clamp mode with an Axopatch 200B amplifier (Axon instruments) controlled by stimfit software with Digidata 1440A interface (Molecular Devices) All recordings were acquired in whole-cell patch clamp configuration. After baseline establishment a glass pipette (1MΩ) filled with 10 mM Met in ACSF was directed to the recording neuron and brief puffs were applied. After application of Met return to baseline was monitored.

2.2.7. Antibody labeling

At DIV15-18 transduced hippocampal neurons were checked for morphological health and channel expression using a fluorescent lamp (EVOS YFP) and were subsequently labeled for immunofluorescence. For staining, neurons were fixed with 4% PFA in 50% (v/v) culture medium for 10 minutes at RT. Cells were washed 3x with PBST (0.1% v/v

Tween, Sigma in PBS) and incubated in permeabilization buffer (0.25% v/v Triton 100x Sigma in PBS) for 20 min at RT. Cells were washed 3x with PBST and incubated with blocking solution (1% BSA Sigma w/v in PBST) for a minimum of 1 h at 37°C. Labeling was carried out in a wet chamber with primary antibodies against GFP (rabbit anti-GFP dilution 1:750, ab290, AbCam), glutamate ionotropic receptor NMDA type subunit 1 (GluN1) (mouse anti-GluN1 dilution 1:100, #114011, Synaptic Systems), glutamate ionotropic receptor AMPA type subunit 2 (GluA2) (rabbit anti-GluA2 dilution 1:500) post-synaptic density protein 95 (PSD-95) (mouse anti-PSD-95 dilution 1:200, #MA1-046, Thermo Fisher Scientific), and microtubule associated protein 2 (MAP2) (guinea pig anti-MAP2 dilution 1:1000, #188004, Synaptic systems) overnight (16 h) at 4°C. Glass coverslips were transferred to a 24-well plate and washed 4x with PBST and transferred back to the wet chamber for incubation with corresponding secondary antibodies (goat-anti-mouse STAR RED, dilution 1:1000, # 2-0002-011-2, Abberior®, goat-anti-rabbit STAR 580 # 2-0012-005-8 , dilution 1:500, Abberior®, goat-anti-guinea pig Alexa Fluor® 488 #A11073, dilution 1:500) for 1 h in the dark at RT. Coverslips were washed 3x with PBS in 24-well plates, washed once with ultrapure water, mounted on micro slides (Assistant) with Mowiol mounting medium and left to dry at RT. For STED imaging samples were imaged within 6 h of mounting.

2.2.8. Imaging

2.2.8.1 TIRF/Confocal microscopy

A Zeiss Axio Examiner Z1 inverted microscope equipped with Plan-Apochromat objectives (10x NA0.45 Air, 20x NA Air and 63x, NA 1.4 oil) was used to image brain slices. Images were obtained with an Ar laser with 514 nm and a PMT detector. A Zeiss inverted LSM 700 confocal microscope equipped with a Plan-Apochromat objective (40x. NA 1.2 Water) was used to image transfected HEK cells expressing GluA2(flop)_eGFP, iMetR and iMetR channel variants with a laser line at 488 nm and acquired with a PMT detector. TIRF images were acquired with an Olympus IX83 microscope equipped with cell^TIRF module. An Olympus UApo oil immersion objective (100x, NA 1.49) was employed to image HEK 293 cells expressing iMetR and GluA2(flop)_eGFP (GluA2_eGFP) in TIRF illumination. An excitation wavelength of 488 nm for mVenus and eGFP was used to obtain images with a quad line beam

splitter emission filter (Chroma) and an EM-CCD camera (Hamamatsu). To assess stable membrane expression live samples were imaged for 120 frames at 1 Hz. All Images were assessed in Image J.

2.2.8.2 STED imaging

Super Resolution images of PSD-95 and GluN1 labeled neurons expressing iMetR and variants were acquired on a commercial STED Microscope (Abberior Instruments) using the Imspector software (Abberior) and equipped with a UPLSAPO 100X Oil objective (Olympus) . iMetR, transduced cells were first identified using a red LED (585 nm) through the eyepiece. Subsequently, co-staining for MAP2 (488 nm) and PSD95 positive spines (640 nm) in confocal microscopy was used to identify dendrites. Two color STED images of PSD-95 and mVenus, GluN1 and mVenus, were acquired using 7.24 µW/561 laser, 15.22 µW/640 laser and 123.4 mW/775 laser (STED) with 6 line steps for each channel. The corresponding confocal images were acquired simultaneously using 7.24 µW/561 laser and 15.22 µW/640 laser with 1 line step for each channel. For both STED and confocal images pixel size was set to 20 nm and dwell time per pixel was 15 µs. Gating time for STED imaging was adjusted to exclude detection of the confocal halo generated by early spontaneous emission. Image analysis 1 and 2 were both performed in Image J Analysis 1 employed the TrackMate plugin to analyze particles.

2.4. Results

2.3.1. Electrophysiological characterization of iMetR in heterologous expression systems

The goal of our study was to develop a receptor with GLR-topology into an orthogonal synthetic neurobiology tool that takes advantage of GLR evolutionary adaptations (Fig 2.1A). In order to determine whether AtGLR1.4 was functionally expressed in mammalian cells without modifications, we transfected HEK 293 cells with a vector encoding for a YFP-tagged version of the protein. We initially examined if we could induce observable current upon bath application of Met in whole cell patch clamp experiments. AtGLR1.4 in oocytes is strongly inwardly rectifying at negative potentials

[63]. Application of 0.1 or 1 mM Met did not result in detectable current, even at very negative potentials (-100mV).

AtGLR1.4 shares structural aspects (see above) with iGluRs, specifically the Ca^{+2} permeable NMDA receptors (NMDAR), which have the highest sequence identity with the ligand binding domain (LBD) of AtGLR1.4 [83]. However, key signaling motifs for the mammalian secretory pathway, which reside in the N and C terminal regions of iGluRs [84-88] are not present in AtGLR1.4 [63, 72]. Previous work on microbial proteins has shown that applying molecular principles to receptors of interested can optimize transcellular trafficking in mammalian cells. This has also been applied to engineered iGluRs [49]. We reasoned that the channel might be retained in one or more subcellular secretory organelles and therefore have low or unstable membrane expression. To address this we optimized AtGLR1.4 by incorporating motifs that encode trafficking signals for excitable cells (Fig 2.1B, C). We replaced the AtGLR1.4 signal peptide with a neuronal nicotinic acetylcholine receptor β subunit (nβAchR) signal peptide and attached a membrane trafficking signal from the inwardly rectifying voltage-gated potassium channel 1.2 (Kir1.2) directly before the stop codon in AtGLR1.4, followed by a mVenus visualization tag. Furthermore, an endoplasmic reticulum (ER) export signal, also from Kir1.2, was placed directly after mVenus with a stop codon (Fig 2.1C). The chimeric channel gene was then further codon optimized for mammalian expression and named iMetR1.0. iMetR1.0 could be easily identified on the membrane of HEK 293 cells both in TIRF microscopy and in confocal microscopy (Fig 2.1D). Time lapse images taken of HEK cells expressing iMetR1.0 in TIRF show stable membrane expression that can be observed with lateral movement in the membrane [89]. In comparing confocal images of GluA2_eGFP with iMetR1.0 we found that iMetR1.0 exhibited enhanced clearing of the ER over that of GluA2_eGFP (Fig 2.1D). However, whole cell recordings of iMetR1.0 were absent of any detectable current in HEK 293 cells upon application of 1 mM Met (data not shown). Furthermore, while Met induced currents were not present we could detect current from cells expressing GluA2_eGFP, suggesting that membrane expression was not the primary reason for the lack of iMetR current.

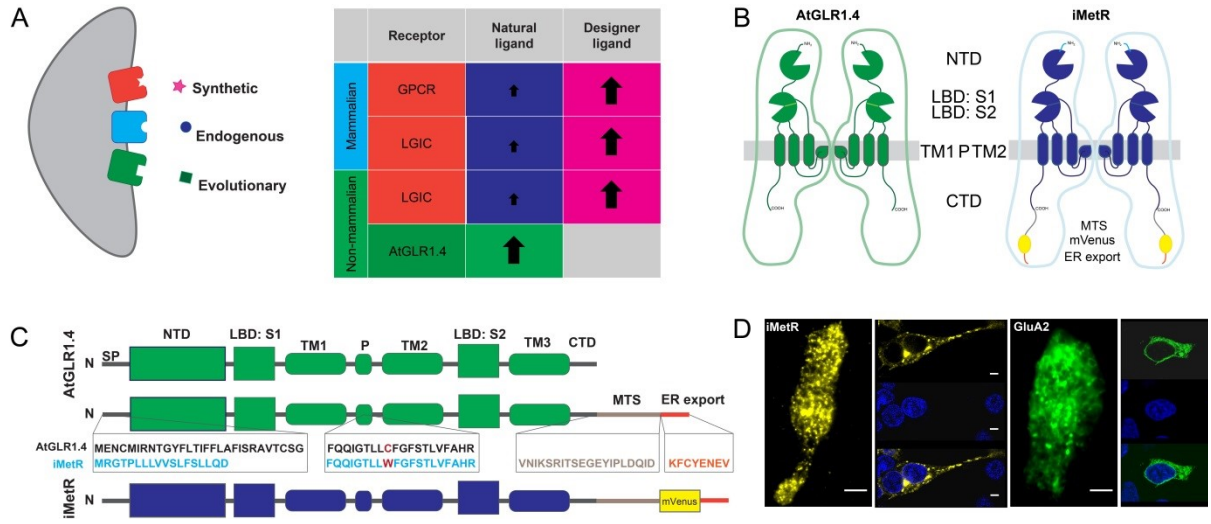

Fig 2.1. Orthogonality and optimization of a plant GLR for mammalian cell membrane expression (A) Concept of evolutionary orthogonality using a plant GLR. (B,C) Cartoon of modified AtGLR1.4 with exchanged and tagged motifs, and pore point mutation (red) (D) iMetR shows enhanced membrane expression in HEK 293 cells compared to GluA2_eGRP (TIRF, 100x), first and third panel; (confocal, 40x), second and fourth panel. All scale bars denote 5 µm.

Previous work in oocytes found current amplitude below 0.1 µA for AtGLR1.4 [63], and this result combined with robust protein expression is indicative of a small single channel conductance and offers a potential explanation for the lack of observable current in HEK 293 cells. We sought to increase channel conductance by introducing a point mutation identified by the Hollmann lab at position 610 from cysteine to tryptophan (AtGLR1.4ΔC610W; Fig 2.1C) that reported a significant increase in current amplitude in oocyte electrophysiological recordings (D. Tapken, unpublished results). Indeed, in oocyte recordings with AtGLR1.4ΔC610W gave current amplitudes around 3.5-fold average current amplitudes at 0.1 (0.32 ± 0.07 mean ± SEM., n = 10) or 1 mM Met (0.35 ± 0.09 mean ± SEM., n = 9) over the reported, with maximum current detected around 1 µA. This mutant was then also employed in mammalian cells. Taking advantage of detectable currents in oocytes and using an automated fast perfusion system [81], we tested whether AtGLR1.4ΔC610W carries the desensitizing characteristics of iGluRs. At an exchange time of around 40 ms (400

µL/s, chamber volume 15 µL) we observed very weak desensitization compared to an engineered GluA2 [90, 91] (τ_{on} 460 ± 54 ms, mean ± SEM., n= 8) (Fig 2.2A).

AtGLR1.4 gating responses to signaling molecules that are present in plants were tested in previous reports [63]. The tested signaling molecules included well known mammalian neurotransmitters (NT), such as glutamate (Glu), glycine, aspartate, dopamine (Dopa) and acetylcholine (Ach). To further deduce if iMetR1.0 would exhibit potency to endogenous mammalian NTs, we also examined whether ɣ-aminobutyric acid (GABA), the major inhibitory NT in the mammalian CNS, induced channel opening We found that the channel was not gated by GABA (Fig 2.2B) and we further confirmed that neither Glu, Ach nor Dopa were effective agonists of AtGLR1.4ΔC610W (Fig 2.2B).

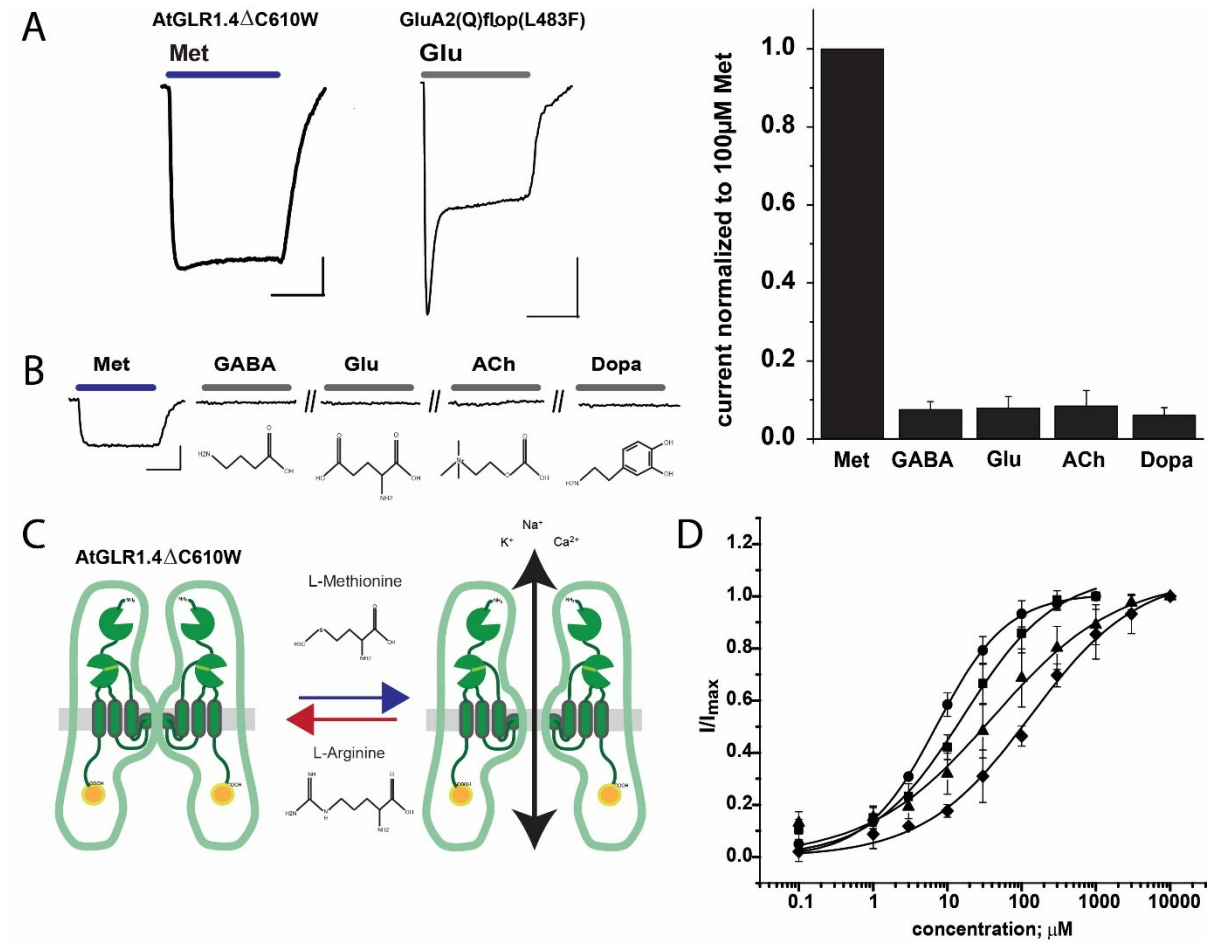

Fig 2.2. Analysis of AtGLR1.4 gating. (A) AtGLR1.4ΔC610W gating response to fast application of Met (0.1 mM) versus gating response of GluA2(Q)flop(L483F) to Glu (0.1 mM) (B) Representative current traces elicited from AtGLR1.4ΔC610W in

response to application of major NTs (0.1 mM for each compound, left), average current amplitudes of NTs normalized to current response from 0.1 mM Met (right bar graph) (C) Cartoon of agonist and antagonists on channel gating (D) Met dose response curve for AtGLR1.4ΔC610W in response to application of 0 (circles),10 (squares), 30 (triangles), and 100 μM (diamonds) Arg. All scale bars represent 0.1 μA and 10 s. Data shown as the mean, error bars denote ± SEM., n = 8 for each condition.

2.3.2. Natural amino acids act as "on/off" switches of iMetR gated currents

In line with its role as an amino acid sensor in plants, a broad spectrum of other natural amino acids act as agonists or even antagonists of AtGLR1.4 [63]. We sought to take advantage of this promiscuous ligand binding profile by identifying a molecule that could endow a natural "off" switch to the channel, in experiments that mimic the pharmacological profile of Met in neuronal tissue. Of the natural amino acids that showed antagonistic behaviour, Arg exhibited the highest potency [63]. Arg is an essential amino acid in the mammalian brain and precursor of nitric oxide [92] yet like Met, Arg is not a molecular component of electrical transmission in the mammalian brain. In order to assess the competitive interaction of Met and Arg on AtGLR1.4ΔC610W we performed Arg dose-response measurements in the presence of Met (Fig 2.2D). Consistent with previous findings for AtGLR1.4, application of increasing concentrations of Arg (0.01 – 0.1 mM; EC_{50} 7.15 ± 0.45, 16.6 ± 4.14, 40.92 ± 11.56, and 131.94 ± 21.81 μM; Hill coefficients 0.9 ± 0.04; 0.7 ± 0.09, 0.52 ± 0.056, 0.6 ± 0.04, respectively, data shown as the mean ± SEM) shifted the Met dose-response curve (Fig 2.2D) demonstrating that Arg is a potent competitive antagonist of Met-induced currents in AtGLR1.4ΔC610W at a wide concentration range.

We went on to validate this result in mammalian cells. We applied the high conductance substitution to the pore domain of iMetR1.0 (position 599 corresponds to the altered position in AtGLR1.4ΔC610W (Fig 2.1C)). We also tested additional substitutions at position 599, including substitutions to serine (Ser), alanine (Ala), histidine (His) or tyrosine (Tyr). These substitutions did not result in detectable current (in the case of Ser, Ala and His) or smaller currents (in case of Tyr; data not shown). A codon optimized version of iMetR1.0CΔ599W was subsequently referred to as

iMetR. iMetR had the same expression pattern in HEK 293 cells as iMetR1.0 and gave detectable current upon 100 µM Met (Fig 2.3A). Next we examined whether Arg would act as a sufficient “off” switch. Upon application of 1 mM Arg we saw an elimination of channel current that could be rescued with an exchange of bath solution containing Met (Fig 2.3A). The current-voltage relationship of iMetR showed sharp inward rectification at negative potentials in whole cell voltage clamp mode (Fig 2.3B) with a reversal potential of 11.7 ± 6.1 mV.

2.3.3. iMetR exhibits graded dose response in a simulated in vivo environment

As mentioned above, AtGLR1.4 has been shown to bind a range of amino acids that are found in their free form in the mammalian brains’ interstitial fluid (ISF). Next, we tested whether these amino acids would inhibit gating by Met *in vivo*. We performed an in depth search of mammalian microdialysis literature to determine the probable concentrations of those amino acids that showed significant potency for AtGLR1.4 in the ISF. We compared these concentrations against the reported EC_{50} and percent inhibition for AtGLR1.4, to determine which amino acids were necessary to test in conjunction with Met gating (Table 2.1). The composition of this custom bath solution, which we referred to as extra-synaptic solution (ESS) comprised mostly of antagonistic amino acids (R, K, V, C, A, H, S, I, Q) and a few agonistic amino acids (M, T, L) (see methods and Table 2.1 for concentrations). We found that application of ESS exhibited the same inhibitory block of the iMetR current as Arg alone when exchanged for normal bath solution (ECS) (Fig 2.3B). When we exchanged ESS with ESS containing a low concentration of Met (0.1 mM) only about 25% (27.5 ± 6.1 data shown as the mean ± SD) of the current could be recovered, yet when we exchanged bath solution for ESS containing a high level of Met (1 mM) around 90% (88.9 ± 10.8 data shown as the mean ± SD) of the Met induced current detected in ECS could be recovered (Fig 2.3 C,D). This finding shows that there is a natural intrinsic block in the mammalian brain that will inhibit any spontaneous channel opening as well as show that a graded acute increase in exogenously applied Met will activate iMetR, in a concentration dependent manner.

The apparent lagged kinetics of iMetRs versus iGluRs in terms of chemogenetic or SNT application will most likely not be a hinderance as Met will not be cleared as

fast as a native neurotransmitter therefore allowing a sustained depolarized state which may coincide with synaptic release events and facilitate modulation of synaptic or neuronal behaviour.

Table 2.1 **[Amino acid] profile in simulated ISF**

Agonist Amino Acid	Brain region	Flow rate (µl/min)	[Microdialysate] (µM)	% of I_{Met}	EC_{50} (µM)	[ESS] (µM)	Source
Met	Hippocampus	2*	6.4	100	7.30 ± 0.55	10	**[93]**
Trp	Cortex	1	3.84	42.5 ± 3.1	49.5 ± 3.1	0	[94] **[95]** [96] [97] [98]
Phe	Hippocampus	2*	8.8	24.4 ± 0.7	103 ± 4	0	**[93]** [95]
Leu	Hippocampus	2*	22	24.0 ± 1.0	31.5 ± 1.8	25	**[93]** [99]
Tyr	Hippocampus	2*	10.4	18.6 ± 1.6	188.9 ± 19	0	**[93]** [98]
Asn	Hippocampus	2*	6.8	18.1 ± 0.5	264 ± 7	0	**[93]** [100] [95] [101]
Thr	Hippocampus	2*	46	13.8 ± 1.2	52.6 ± 1.4	50	**[93]** [100]
Norleucine	n/a	n/a	n/a	16.5 ± 0.8	26.4 ± 3.5	(excluded****)	n/a

Antagonist Amino Acid	Brain region	Flow rate (µl/min)	[Micro dialysate] (µM)	% of 0.1 mM I_{Met}	% of 1 mM I_{Met}	[ESS] (µM)	Source
Arg	Hypothalamus	1.5**	122**	80	48	150	[94] [95] **[102]**
Gln	Hippocampus	2*	651*	78	32	650	[93, 94] [100] [95] [101] [103] [104] [105] [99]
Lys	Hypothalamus	1.5**	450.4**	68	23	450	[95] **[102]**
Val	Hippocampus	2*	22.8	55	18	25	**[93]** [101]
Ile	Hippocampus	2*	10.4	50	15	15	**[93]**
His	No data found	No data found	No data found	50	12	50***	**[106]**
Cys	Cortex	2*	3.84	48	10	5	**[107]** [98]
Ala	Hippocampus	2*	42	40	8	45	[94] **[93]** [100] [95] [101] [103] [102] [99]
Ser	Hippocampus	2*	69.9	15	3	70	**[93]** [100] [95] [103]

Microdialysate concentrations are shown as the mean plus one standard deviation. Concentrations included in ESS represent a rounded number from microdialysate for convenience purposes. All amino acid concentrations with the exception of histidine were acquired from literature using *in vivo* microdialysis (source in bold). In the case where there was a range of concentrations for an amino acid, the upper limit concentration was applied.

*[aa] in dialysate was multiplied by a factor of 40 on the basis that the recovery rate for amino acids *in vitro* was 5% for the dialytrodes used in the study. Data was adjusted on the recommendation of the authors to account for a 50% recovery rate of *in vivo* for chronic implants in anesthetized animal [93].

** awake behaving animals, in vitro recovery rate 5-10%, lower recovery limit was taken [102]

*** no microdialysis data available - included due to precursor to histamine

**** no microdialysis data available - excluded

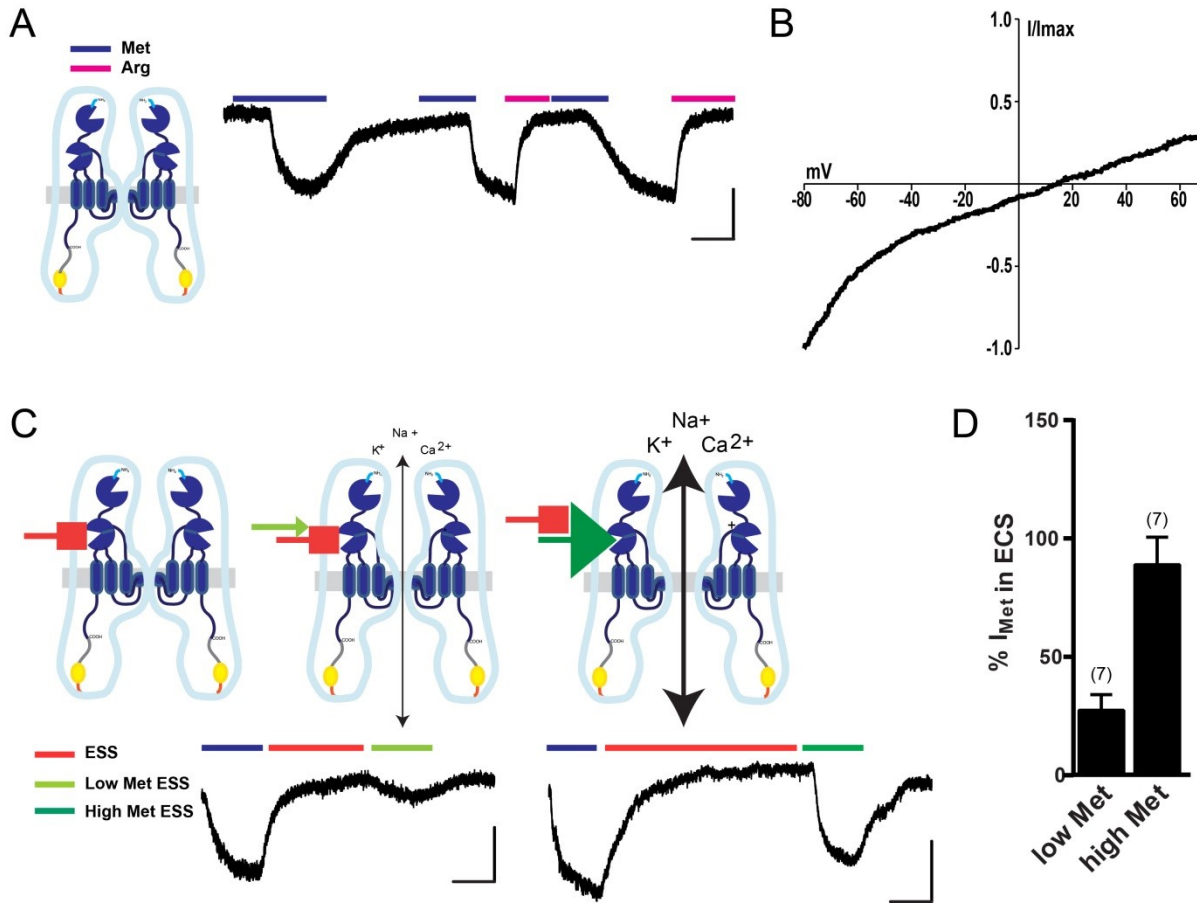

Fig 2.3. Natural amino acids act as an "on/off" switch in HEK 293 cells expressing iMetR and graded responses in a simulated *in vivo* environment

(A) Activation of iMetR with Met (0.1 mM) which is reversed with Met wash out or blocked by Arg (1 mM) wash in (B) Met induced current-voltage relationship (ramp from -80 - + 80 mV), currents were normalized to the maximum amplitude at -80 mV (n=3). (C) Cartoon of amino acid profile on iMetR with bath exchange of ESS (above), iMetR representative whole cell current traces in HEK 293 cells in application to ESS, ESS with low Met (0.1 mM), or high Met (1 mM) (D) iMetR current is reduced in ESS with low Met and recovers in ESS with high Met (1 mM), shown as percent of Met current responses in normal bath solution (0.1 M Met) (n is represented above each condition). Cells were held at -70 mV in whole cell voltage clamp mode. Data shown as the mean, error bars denote ± SD., all scale bars represent 0.05 nA and 50 s

2.3.4. iMetR variants with C-terminal post-synaptic targeting motifs

After demonstrating the suitability of iMetR for manipulation of neuronal electrical signals with respect to ligand binding and ion conduction properties, we further modified the protein for functional enhancement in neurons. We reasoned that transferring signaling motifs from proteins that localize post-synaptically would increase site directed expression of iMetR and, due to the slow kinetics of the channel, an increase in retention at post-synaptic sites may enhance the modulation of post-synaptic potential. We therefore engineered two C-terminal motif variants, one that replaced the C-terminus (CT) of iMetR with that of GluA2 (iMetRΔR2ct) and one that incorporated the last 15 amino acids from stargazin (ɣ2) directly after the CT which contains the PDZ binding domain (iMetRɣ2$_{15}$) (Fig 2.4A). Confocal images for both variants expressed in HEK 293 cells show expression patterns similar to that of iMetR (Fig 2.4B). Surprisingly, iMetRɣ2$_{15}$ showed 3-fold increase in current whereas iMetRΔR2ct currents were comparable to iMetR (Fig 2.4C, D). We reasoned that this may be due to an increased channel conductance or an increase in membrane expression of iMetRɣ2$_{15}$. Because both of these properties are known to be modulated by ɣ2 [108-110] we tested whether co-expressing ɣ2 and iMetR or iMetRΔR2ct would result in the same effect on current amplitude.

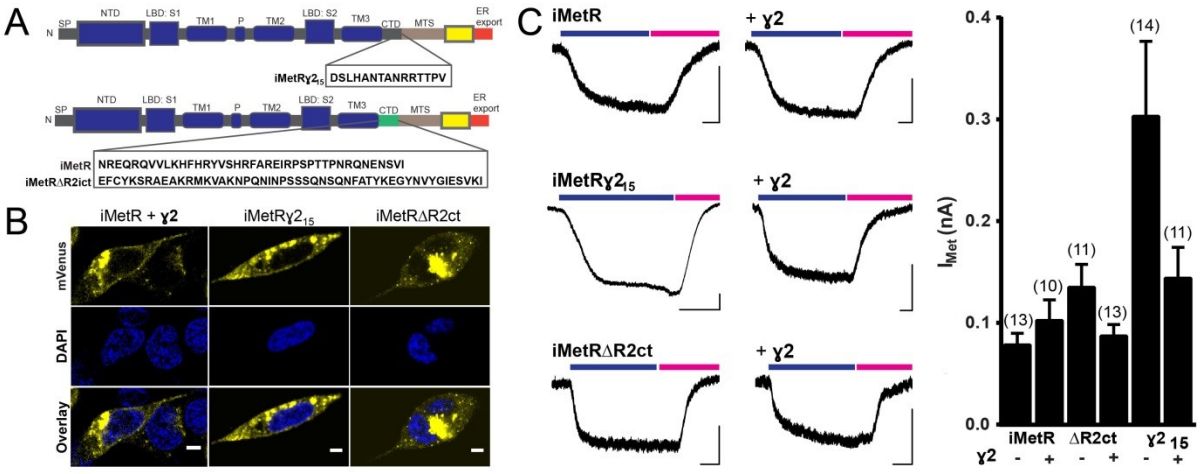

Fig 2.4. Tagging iMetR with a post-synaptic density retention signal conveys increased channel conductance (A) Cartoon of iMetR CT modifications (B) Confocal images of iMetR co-expressed with ɣ2 (left panel), iMetRɣ2$_{15}$ (middle

panel), and iMetRΔR2ct (right panel) (C) representative currents from HEK 293 cells expressing iMetR, iMetRγ2$_{15}$, and iMetRΔR2ct co-transfected with empty vector (left) or γ2. Cells were held at -70 mV in whole cell voltage clamp mode. Scale bars represent 0.1 nA and 20 s. Data shown as the mean, error bars denote ± SEM., n is represented above each condition.

It was a surprising that iMetRΔR2ct did not exhibit an increased current amplitude with γ2 co-expression (Fig 2.4D) as it is the variant that contains the most enhanced form of iGluR trafficking and complexing signals. One likely explanation is that this channel variant is already efficiently targeted to the membrane.

2.3.5. iMetRΔR2ct co-localizes with NMDA receptors but shows no preference for post-synaptic densities

Next, we investigated iMetR expression in neurons both *in vitro* and *in vivo*. Upon transduction of dissociated hippocampal cultures using lentivirus we found that all variants showed good membrane expression (Fig 2.5). We further sought to determine whether the additional tags normally associated with post-synaptic densities would increase localization of the channels in a synapse specific manner. We employed immunolabeling and 2-color stimulated emission depletion (STED) microscopy to assess whether iMetR channels localized with PSD-95 signals and therefore are likely present in post-synaptic densities. We also tested for localization with GluN1, the necessary subunit in N-methyl-D-aspartate receptors, to determine whether there was spatial overlap with endogenous iGluRs independent of PSD. For image analysis 1 (Fig. 2.5 D) of overlapping iMetR puncta with PSD-95, the lower limit area restriction for PSD-95 was set at 10 nm^2 [111, 112] and no upper limit restriction. We used these parameters to distinguish synaptic regions. We did not discriminate in location of NMDAR densities due to the difficulty in discriminating between localized channels, those in transit, and those waiting for recruitment [113]. We found that there was overlap in all channels with PSD-95 yet no discernable difference between iMetR, iMetRΔR2ict, or iMetRγ2$_{15}$ (Fig 2.5 D-F). Inclusion of GluA2 densities and restriction of PSD-95 puncta set at a between 10 - 540 nm^2 using analysis 2 (Fig 2.5 L) We found

that there was overlap in all channels with PSD-95 but a significant difference between GluA2, iMetRΔR2ict, or iMetRγ2$_{15}$ and iMetR (Fig 2.5 G-K). This indicates the importance of

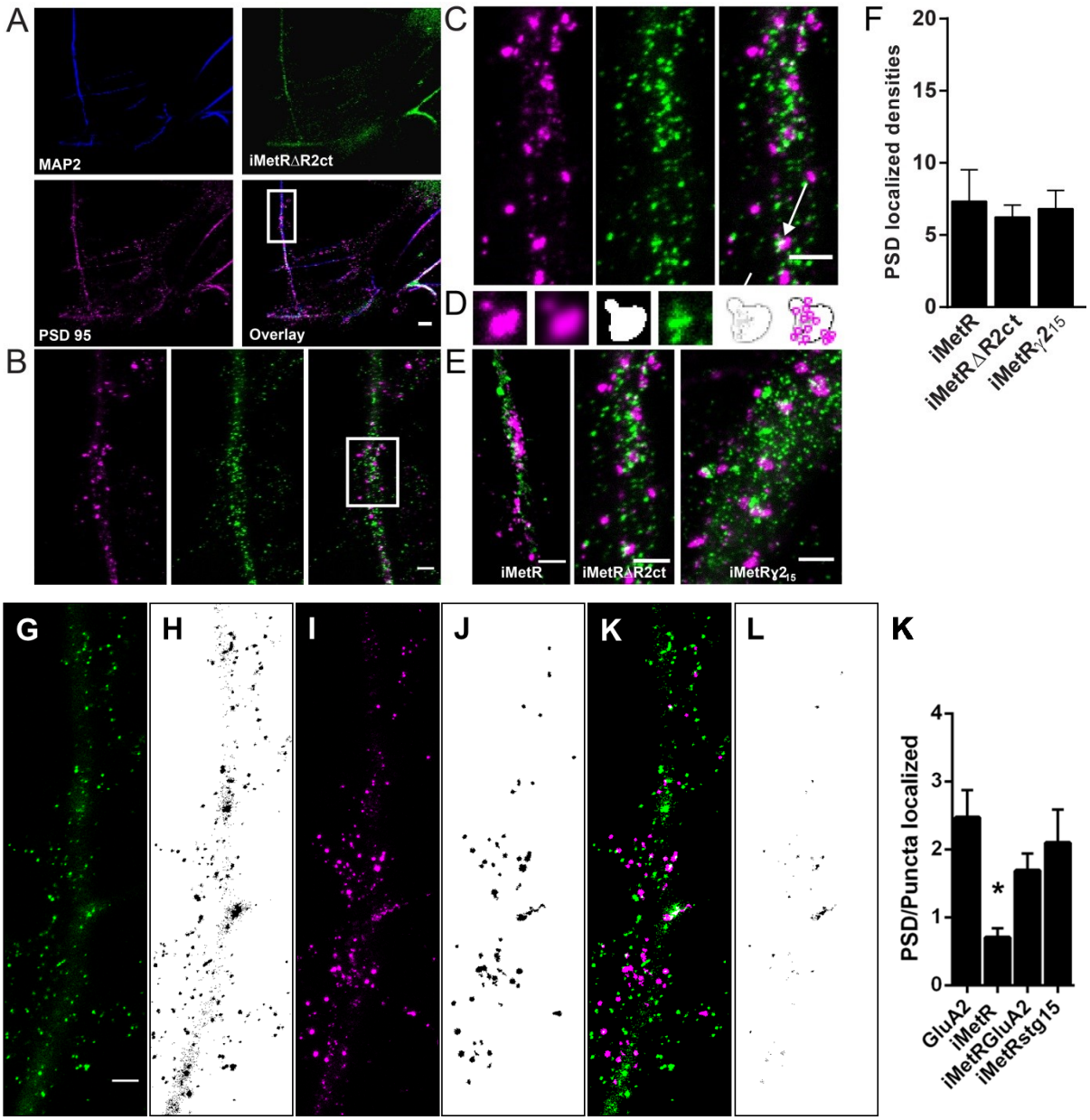

Fig 2.5. 2-color STED reveals iMetR localization to post-synaptic densities in hippocampal neurons (A) Representative confocal images of dendritic (MAP2) and post-synaptic density (PSD-95) markers in a hippocampal neuron expressing iMetRΔR2ct, overlay image boxed where STED was applied. (B) STED resolved image of PSD-95 (magenta) and iMetRΔR2ct (green), boxed image in overlay is a

representative section that was enlarged for analysis (C, D). Images were analyzed separately, endogenous staining was blurred using a Gaussian filter, sectioned into binary spots and subtracted from iMetR channels (green) using TrackMate, particles within defined regions were counted as localized to PSD-95. (E) Representative pictures of iMetR channel variants overlaid with PSD-95. All identified PSD-95 regions and iMetR puncta were averaged over the number of PSD-95 regions with the same image (D, E, F). GluA2 puncta (G) and removal of the background to show GluA2 puncta for localization (H), PSD-95 puncta (I) and puncta after background removal and size restriction (J). GluA2 and PSD-95 overlay (L) show those regions in white are identified as GluA2 particles found within PSD-95 puncta (K). Analysis 1 n = 135, n = 1570, and n = 757, for iMetR, iMetRΔR2ct, and iMetRγ2$_{15}$ respectively, n represents PSD-95 puncta over 2-8 images. For analysis 2, n = 478, n = 25, n = 642, n = 1648 for GluA2, iMetR, iMetRΔR2ct, and iMetRγ2$_{15}$ respectively, n represents overlay particles over 2-13 images. Data shown as the mean, error bars denote ± SD. * = $p < 0.05$, two-tailed t-test with Welch's correction.

We did observe a significant difference in the localization of iMetRΔR2ct with GluN1 over that of unmodified iMetR using analysis 1 from above (Fig 2.6) with no restrictive limits for the reasons stated above on channel particles. Due to the nature of introducing exogenous proteins as well as the phenomena of synaptic scaling [114, 115] iMetRΔR2ct may compete with native GluA2's for slots in the PSD, which could be an explanation for why we found no preference for iMetRΔR2ct over iMetR in PSD-95 localized areas

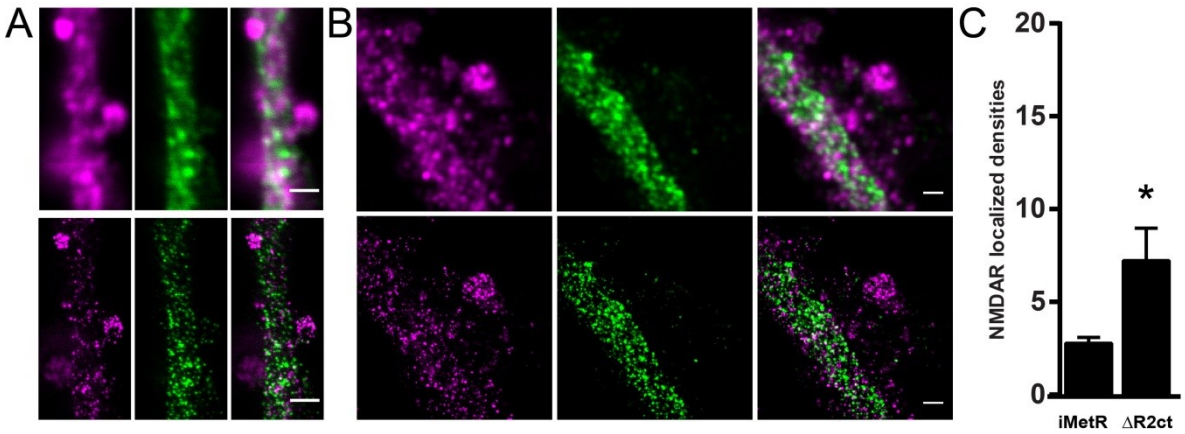

Fig 2.6. iMetRΔR2ct exhibits preferential targeting to iGluR "slots" Representative images in Confocal (top panels) and STED (bottom panels) resolution of hippocampal dissociated culture labeled against GluN1 subunit (magenta) and mVenus (green), dendritic structures expressing (A) iMetRΔR2ct or (B) iMetR. (C) iMetRΔR2ct shows a significant increase in localization with GluN1 over iMetR. Data shown as the mean, error bars denote ± SD., n = 1156 and n = 532 for iMetR and iMetRΔR2ct, respectively, n represents NMDAR puncta over 7-9 images * = $p < 0.05$, two-tailed student's t test.

In addition, all variants of iMetR showed high expression when virally expressed in the dorsal dentate gyrus (DG) of mice. iMetR expression was compared to either iMetRΔR2ct or iMetRγ2_{15} by unilateral expression into the left hemisphere for iMetR and one variant into the right hemisphere of the same animal. Expression was assessed after 15 d with confocal microscopy (Fig 2.7).

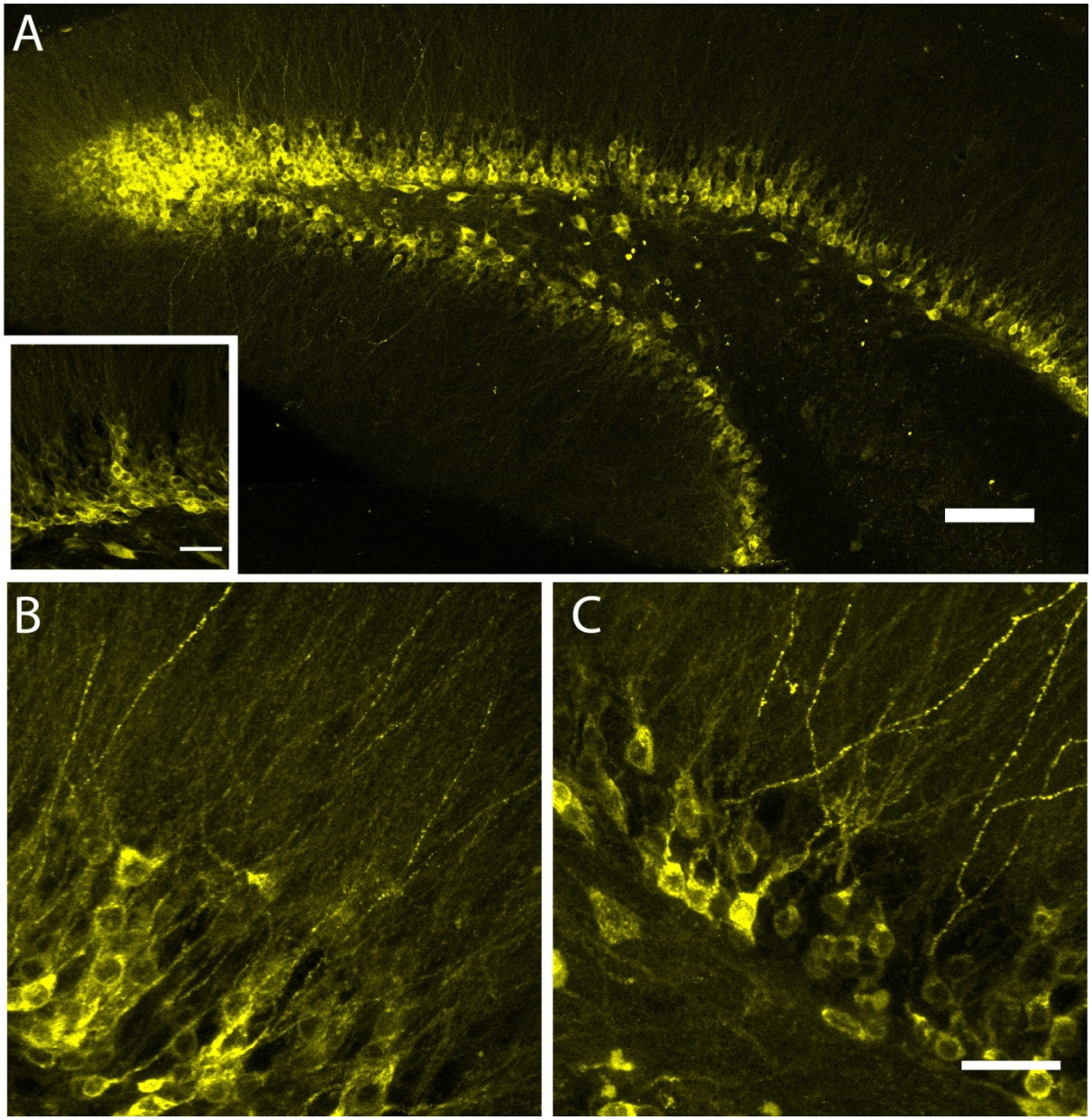

Fig 2.7 iMetRs express *in vivo* in the dorsal DG of mice (A) iMetR (10x) scale bar represents 100 μm, insert scale bar represent 10 μm (40x) (B) iMetRγ2$_{15}$, and (C) iMetRΔR2ct, (40x) scale bars represent 10 μm.

We performed slice electrophysiology on dentate granule cells that exhibited expression of iMetRγ2$_{15}$ due to the increased amount of current observed in HEK 293 cell and preferential spine localization determined by 2-color STED. Application of Met using a guided pipette onto the cell body induced specific depolarization steps depending on the length of application (Fig 2.8 A) but did not induce action potentials.

However, application of Met to the dendritic arbor did induce action potential firing suggesting that iMetRɣ2$_{15}$ expression in neurons with a combination of increased channel current and subcellular retention is sufficient to initiate action potentials. Further electrophysiological experiments are required to determine whether and to what extent somatic versus dendritic Met application effects the depolarizing state of neurons expressing iMetRɣ2$_{15}$.

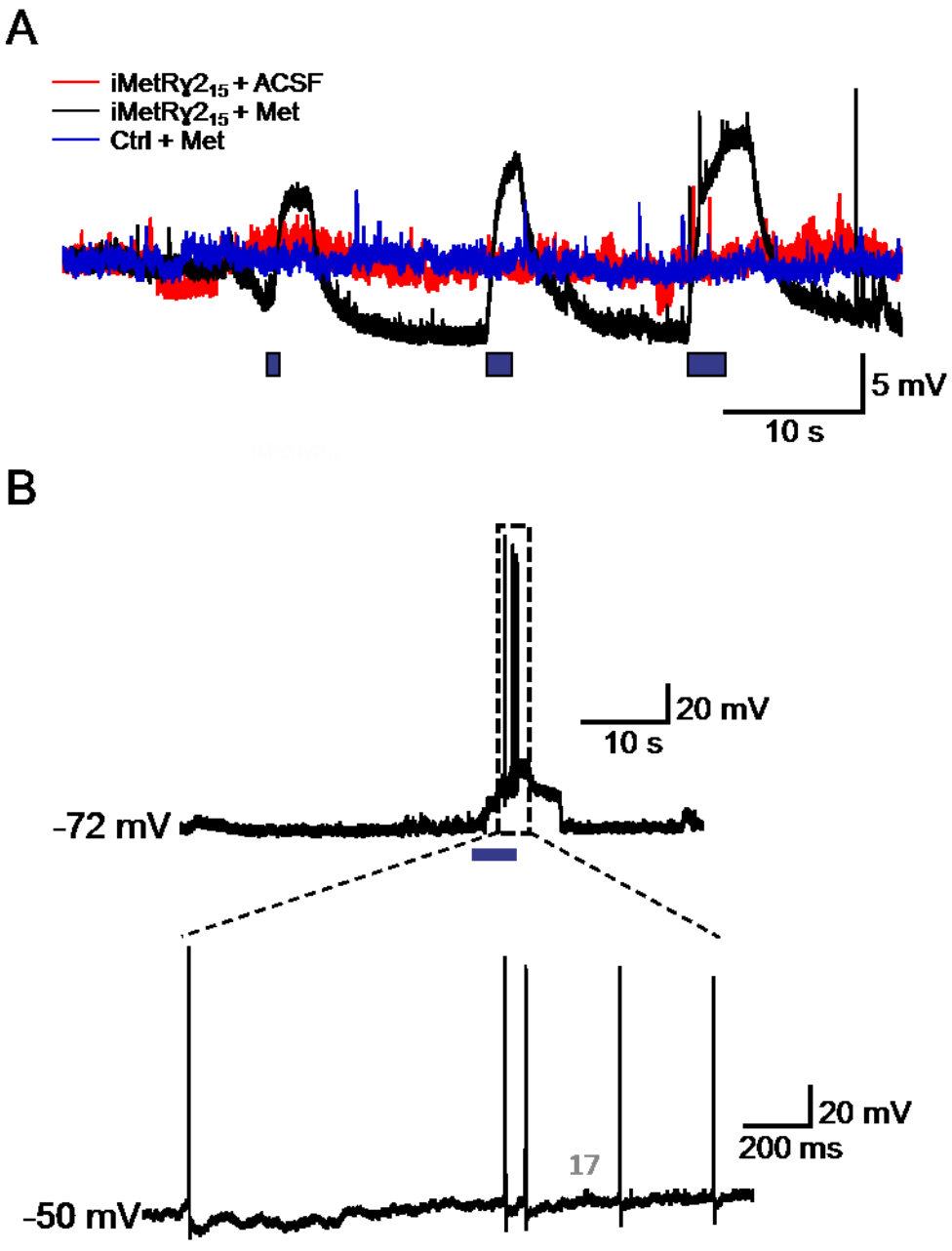

Fig 2.8 Subcellular Met application of iMetRɣ215 induced action potentials in Hippocampal neurons (A) Somatic Met puff induced membrane depolarization which was not observed with ACSF puff on iMetRɣ2_{15} expressing neurons or untransduced neurons in the same layer with Met application (B) Dendritic Met puff induced action potentials on neurons expressing iMetRɣ2_{15}. Each trace represents an n = 1.

2.5. Discussion

The past two decades have seen a paradigm shift in neuroscience research with the advent of genetically encoded tools that allow researchers to manipulate neuronal communication in a cell type-specific manner. Existing chemogenetic techniques exclusively rely on ligands that are non-natural but designed to activate engineered receptors. Non-natural designer ligands pose specific concerns in terms of ligand clearing (no endogenous system in place) and orthogonality (reactivity with un-targeted receptors) that could lead to possible off target effects including unrealized circuit or system-wide gain of function. We have, in part, addressed these limitations by identifying a natural ligand – receptor pair where the ligand retains its natural properties and in which the system has native housekeeping abilities for, while acting orthogonally in a mammalian system and specific activation of its receptor.

Ion channels are ideal receptors to employ in a chemogenetic strategy because they directly control ion fluxes, which can be further tuned by means of engineered pore properties. We re-purposed a plant GLR to induce bioelectric signals in mammalian cells with the ultimate goal of modulating excitable cells, by its natural ligand. The three clades of GLRs expressed in *A. thaliana* share similarities both in structural topology and functionality with mammalian iGluRs. Specifically, AtGLR1.4 is a mixed cation channel from the clade 1 family, notably permeable to calcium that has been well characterized in the heterologous system oocytes from *X. laevis*.

iMetR is an attractive candidate chemogenetic tool because of the properties of its primary ligand Met (e.g. low toxicity, inexpensive, BBB permeability, and a common PET tracer). As with any biochemical tool, there are considerations to the use of natural aminos as “designer” ligands. Both Met and Arg are known to be neuroprotective amino acids [116-119] and off target affects may confer

neuroprotective qualities that could be beneficial in counteracting damage done during experimental procedures (e.g. viral injections).

We optimized this channel for mammalian cells, using combinatorial molecular modification to assist channel trafficking through secretory pathway for plasma membrane insertion. Inspired by previous work, we attached motifs for ER export and inserted a mammalian signal peptide. The engineered receptor iMetR exhibited enhanced ER clearing compared to the that of AtGLR1.4 (not shown) and GluA2, which allowed us to conclude that exchanging or adding small peptides, also in this case, assists non-mammalian proteins through a mammalian secretory path to membrane insertion. Additional enhancement can be applied, like those for trafficking out of the Golgi by seamless fusion of a Golgi export signal directly after the signal peptide [73]. However, expression of iMetR and iMetR variants both *in vitro* and *in vivo* lead to satisfactory membrane expression in the absence of this signal as shown by detectable currents upon Met application during whole cell patch clamp recordings in HEK 293 cells (*in vitro*) and microscopy (STED *in vitro* and confocal *in vivo*).

Uniquely, this channel shows competitive antagonistic binding by amino acids other than its dominant agonist Met. Consequently, an “on/off” switch in the form of Met (on) and Arg (off) can be realized as a means to induce sharp or graded responses of bioelectric components in mammalian cells. Upon realizing this antagonistic behavior, we hypothesized that this may lead to an intrinsic block *in vivo* due to the range of amino acids that act antagonistically and are found as “free” in the ISF. We found that applying an artificial ISF named ESS, containing those amino acids that have significant potency profiles for AtGLR1.4 could sufficiently override Met gating. Yet, increasing the levels of Met in the ESS could efficiently rescue the Met-induced current at different levels compared to Met in a conventional bath solution or during system ‘loading’.

In line with the concept of SNT, we created a number of iMetR variants with the goal to retain or accumulate the receptor in critical post-synaptic locations. Following literature on transmembrane AMPAR regulatory proteins (TARPs), we choose to first swap the entire CT of iMetR for that of GluA2. This decision was based on the following criteria. 1. The alignment of iMetR with that of all GluRs that are retained in the post-synaptic density had no conserved residues [72], which implied that while expression may be universal, competition for space within the PSD would be low. 2. We reasoned

that an exchange of the CT for GluA2, which is the most abundant of the AMPAR subunits [120], would mimic AMPAR trafficking and retention in the PSD of excitatory synapses, which is the primary target site for proof of concept tests. In addition, and in line with the above, tag of a singular PDZ binding domain would be an alternative strategy to retain iMetRs in excitatory synapses without the selective GluA properties accompanying a full CT exchange. ɣ2 is a TARP that plays an active role in retention of proteins at the PSD. More specifically, ɣ2 interacts with PDZ domains of the post-synaptic scaffolding protein PSD-95 [121]. We therefore took those 15 amino acids involved in PSD-95 binding, and added them between the end of the CT of iMetR and the membrane trafficking signal. In line with this hypothesis we used high-resolution imaging to determine if swapping CT would indeed show greater localization of iMetR and if the same held true for $ɣ2_{15}$ meant to confer direct facilitation with PSD-95. 2-color STED imaging revealed that while iMetRs did localize to the PSD there was no preference for one over the other. However, the CT exchanged version did show enhanced localization with NMDARs. The observation that all iMetRs exhibited similar localization within regions containing PSD-95 may be explained by ubiquitous expression patterns due to the nature of channel overexpression.

It has been speculated that an elongation of a PSD-95 binding domain may encounter less competition from other transmembrane proteins known to bind to PSD-95 [122]. Therefore a simply elongation of the CT of iMetRΔR2ct with the same ɣ2 PZD domain could further enhance retention in desired slots in the PSD due to the greater availability of PSD-95 slots deeper into the cytoplasm at synapses. Surprisingly, we found that the addition of $ɣ2_{15}$ conferred directly modulation of the channel and resulted in an increase of channel conductance and may be transferrable to iMetRΔR2ct. Due to the range of mobility and interactions between GluA2, ɣ2 and PSD-95 more conclusive STED imaging with endogenous GluA2 and PSD-95 in comparison to iMetR variants will be telling in how representative these iMetR variants are in relation to PSD-95 are in terms of preferential localization. Unlike in the case of other orthogonal ion channel systems that also assemble into oligomers, GLRs are not mammalian proteins and it is thus unlikely that unwanted protein-protein interactions with endogenous ion channels of the same superfamily will occur. Nevertheless, GLRs have retained enough structural topology to enhance channel qualities. GLRs including AtGLR1.4 receptor LBDs have been shown to gate pores

and pore loops of members of iGluRs in chimeric proteins [123]. Taking further advantage of these functional similarities the possibility exists of constructing a K^+ selective receptor through the incorporation of a K^+-selective pore, such as that from GluR0 [55, 124].

Typically chemogenetic tools that are excitable often run into applicative problems like excitotoxicity owing to the fact that the off stage is reliant on clearing of a non-natural ligand. This may be addressed for a natural ligand like Met as there are uptake processes already there to clear it from the active cleft. These processes include metabolic pathways [125] as well as transporters for neutral amino acids (see chapter 4). These findings, in conjunction with the permeability of iMetR to calcium could be a way to apply remote synaptic plasticity paradigms in behaving animals. Overall, the specialized features of iMetR (structural topology, Ca^{+2} permeable, natural amino acid profile, and no reactivity to native NTs), as well as the pharmacological profile of Met and Arg, is a promising tool for neuronal modulation to address a range of modulatory behaviors. Initial characterization of the iMetRɣ215 variant showed promise in applying iMetRs for cellular or subcellular override of neuronal communication. Further electrophysiological experiments in acute slice preparation will be telling to what extent Met-iMetR, iMetRΔR2ct, and iMetRɣ2_{15}, will affect overall neuronal output and to what degree this ligand-receptor combination can be applied *in vivo*.

Chapter 3: Isolation of Synaptic Vesicles from Genetically Engineered Cultured Neurons

I would like to thank Miroslava Spanova for her help in establishing synaptic vesicle isolation and Western Blot analysis. Alexander Johnson for assistance with TIRF microscopy and contribution to image analysis. Stephanie Kainrath for assistance with Western Blot analysis and Harald Sitte (Medical University of Vienna, Center for Physiology and Pharmacology, Institute of Pharmacology) for graciously allowing me to use his lab space and equipment as well his input to the design of uptake experiments. We would in addition like to thank K. Jaentsch for technical assistance, U. Bezeljak for assistance with imaging, M. Freissmuth and H. Drobny for discussions, and M. Sixt, P. Jonas, T. Oertner and T. Rose for vectors and genes.

Text of this chapter is reproduced from: Catherine McKenzie, Miroslava Spanova, Alexander Johnson, Stephanie Kainrath, Harald Sitte and Harald Janovjak (2018) Isolation of Synaptic Vesicles from Genetically Engineered Cultured Neurons J. Neurosci. Meth. in revision.

3.1. Abstract

Synaptic vesicles (SVs) are an integral part of the neurotransmission machinery, and isolation of SVs from their host neuron is necessary to reveal their most fundamental biochemical and functional properties in *in vitro* assays. Isolated SVs from neurons that have been genetically engineered, e.g. to alter protein content or introduce genetically encoded reporters, are not readily available but would permit new insights into SV structure and function. Furthermore, it is unclear if cultured neurons can provide sufficient starting material for SV isolation procedures. Here, we demonstrate an efficient *ex vivo* procedure to obtain functional SVs from cultured rat cortical neurons after genetic engineering with lenti virus. We show that ~$10^{(8)}$ plated cortical neurons allow isolation of suitable SV amounts for detailed functional and biochemical analysis. We found that SVs isolated from cultured neurons have comparable neurotransmitter uptake as SVs isolated from intact cortex. Using total internal reflection fluorescence (TIRF) microscopy, we visualized an exogenous SV-targeted marker protein and demonstrate the high efficiency of SV modification. Obtaining SVs from genetically engineered neurons currently generally requires the availability of transgenic animals, which is constrained by technical (e.g. cost and time) and biological (e.g. developmental defects and lethality) limitations. These results demonstrate the genetic modification and isolation of functional SVs using cultured neurons and viral transduction. The ability to obtain SVs from genetically engineered neurons will permit linking *in situ* studies to *in vitro* experiments in a variety of genetic contexts.

3.2. Introduction

Synaptic vesicles (SVs) are small (~40 nm diameter) secretory organelles that are concentrated at the periphery of active zones in neurons and play an integral part in synaptic communication. SVs harbor proteins that are essential for the packaging of specific neurotransmitters (NT), for positioning of diverse SV populations within the synapse and for SV fusion, in many cases in collaboration with cytosolic and cell membrane-localized protein binding partners [126-128]. SVs have in the past decades become classical models for the study of secretory organelles, and the alteration or

breakdown of their function lead to severe physiological consequences, including motor, neurodegenerative and neurological disorders [129-132].

In line with their vital functions, a plethora of experimental techniques have been developed to study all aspects of SV biology. SVs isolated from rodent brain tissue are the most common preparation to investigate SV protein composition and the specificity and energetics of NT uptake [133-135]. SVs are routinely visualized *in situ* in neuronal cultures and brain slices to study trafficking, fusion and recycling using fluorescent chemical markers, genetically encoded fluorescent probes and false fluorescent neurotransmitters [136-139]. Employing these techniques *in vivo* allows cellular and circuit dynamics to be investigated [140-143]. Finally, advanced microscopy techniques, such as total internal reflection fluorescent (TIRF) microscopy, offer complementary avenues to study isolated SVs and have been applied to detect variability in composition and energetics with single vesicle resolution [133, 144]. In the future, correlating biochemical and bioenergetic properties, which are obtained from the study of isolated SVs, with dynamic and functional properties, which are obtained from *in situ* observations, will likely yield new and fundamental insights into SV biology and synaptic function in health and disease.

One of the most powerful strategies of inquiry across experimental biology is genetic perturbation. Overexpression or elimination of proteins of interest or delivery of genetically encoded functional probes are invaluable tools to understand cellular processes including those involving SVs [145, 146]. It is noteworthy that the application of genetic perturbation in experiments with isolated SVs has been limited [144, 147-149]. One major reason for this gap is that obtaining SVs from genetically modified neurons currently requires the generation of transgenic animals [144, 148, 149]. Generation and maintenance of transgenic animals is costly and hampered by the fact that manipulation of many proteins associated with SV function result in developmental defects or lethality [149-152]. We reasoned that a method for SV isolation from cultured neurons would allow researchers to employ genetic engineering techniques *ex vivo*, including virus transduction, and to focus on specific brain areas or even specific neuronal populations. In two studies [147, 153], SVs were isolated from cultured neurons, which in one case had been transduced with a virus. However, the ability of the purified SVs to take up NTs was not demonstrated and details of the

experimental methodology, such as the amount of starting material or centrifugation protocols, were not disclosed.

Here, we demonstrate that functional SVs are accessible from genetically engineered cultured cortical neurons in suitable amount for NT uptake and biochemical analysis. We showcase the introduction of an exogenous protein into SVs following this method by visualization of single SVs with TIRF microscopy. Collectively, these results demonstrate efficient modification of functional SVs using cultured neurons and viral genetic engineering, and open the door to new structural and functional studies of SVs in diverse contexts.

3.3. Methods

3.3.1. DNA constructs

Ratio1XsypHy was a gift from Thomas Oertner and Tobias Rose and obtained from Addgene (#44268) [138]. Ratio1XsypHy was subcloned into a modified pLenti6.3/V5-DEST vector (Thermo Fisher Scientific) between ClaI and XbaI restriction sites and expressed under the control of the human synapsin promoter (pLenti6.3::hsyn::Ratio1XsypHy).

3.3.2. Lenti virus production (reproduction from chapter 2 with modifications)

Lenti virus production and purification was performed as described previously [78]. 7.0 x 10^6 Lenti-X 293T cells (Clontech) were seeded in Dulbecco's modified Eagle's medium (Life Technologies) supplemented with 10% v/v fetal bovine serum (FBS) in poly-*L*-ornithine (0.01% w/v, Sigma)-coated 15 cm cell culture dishes (Corning) and incubated at 37°C in a 5% CO_2 atmosphere. After 15 h, medium was changed and cells were incubated at 37°C for 30 min. Cells were then transfected with pLenti6.3::hysn::Ratio1XsypHy, VSV-G and delta 8.7 packaging plasmids at a 1:1:1 molecular ratio (total amount: 22.5 μg per dish) with polyethyleneimine (Polysciences) in Opti-MEM I medium (Gibco). Medium was changed after 7 h. 40 to 48 h after transfection, supernatant was collected for centrifugation at 1,000 x g for 10 min followed by filtering (0.45 μm). For virus concentration, filtered supernatant was layered over a 10% v/v sucrose cushion (20% w/v sucrose in 1 M NaCl, 20 mM HEPES, 0.25 mM EDTA, pH 7.4) and centrifuged at 4°C for 1.5 h at 150,000 x g.

During the 2 to 4 separate centrifugation runs, pellets were consolidated, resuspended in culture medium (see below) and stored at 4°C. After centrifugation, concentrated virus was aliquoted into O-ring conical tubes, snap frozen and stored at -80°C. Physical titer was determined using a reverse transcriptase qPCR kit following the provider's protocol (Genecopia). Each viral preparation was tested for functional expression with a dilution series in glass bottom 24-well plates containing 5.0 x 10^5 cortical neurons/well. Expression was assessed daily 5 d after transduction using an EVOS FL microsope (Thermo Fisher Scientific). The virus concentration that produced the highest expression in morphologically healthy cells at day *in vitro* (DIV) 15 was then utilized for transduction of neurons in 15 cm dishes (see below).

3.3.3. Primary cortical neuron culture

Cortical neurons were prepared from batches of six P0-P1 pups of Wistar rats (Janvier Labs). Animal housing and tissue extraction were performed in accordance with national and European guidelines. Briefly, cortices were isolated from both hemispheres in Hank's balanced salt solution (supplemented with 2.5 mM HEPES, 35 mM D-glucose, 4 mM $NaHCO_3$, pH 7.4) by removing midbrain, cerebellum and olfactory bulb and clearing the meninges from the tissue. Cortices were minced with a razor blade and transferred between two 15 ml conical tubes. Dissociation was carried out using a papain dissociation system following the provider's protocol (Worthington). Neurons were maintained following established protocols [79] with modifications. Cells were suspended in plating medium that consisted of modified Eagle's medium supplemented with 10% v/v FBS, 0.6% w/v *D*-glucose, 6 mM GlutaMAX, 1 mM Na-pyruvate, 100 U/ml penicillin and 0.1 mg/ml streptomycin. Cells were counted in a Neubauer chamber and 30 x 10^6 cells were seeded in each poly-*L*-lysine (PLL, 0.1% w/v, Sigma)-coated 15 cm cell culture dish. After 5 to 6 h, one volume of medium (Neurobasal-A, supplemented with 2% v/v B27 and 6 mM GlutaMAX) was added to each dish. At DIV2 to DIV3, medium was supplemented with 4 μM cytosine β-*D*-arabinofuranoside to reduce glial growth. Finally, cells were transduced with lenti virus during medium change at DIV5 and subsequently half of the medium was changed every 2 to 3 d. Neurons were typically transduced with 100 to 150 μl of concentrated virus solution (~0.5 to 0.75 x 10^9 viral particles/dish) and displayed robust expression at DIV15.

3.3.4. SV isolation

3.3.4.1. Culture

Neurons at DIV15 to DIV18 were washed twice with ice cold phosphate buffered saline (PBS). All steps were performed on ice or at 4°C. Homogenization buffer (0.32 M sucrose, 1 mM $NaHCO_3$, 1 mM Mg-acetate, 0.5 mM Ca-acetate, cOmplete protease inhibitor cocktail (Sigma), pH 7.2) was added to a final volume of 5 ml per dish and cells were gently scraped off and pooled in a 40 ml Dounce tissue grinder (Sigma). Homogenization was performed manually with five strokes using pestle A (clearance 0.0030-0.0060") and 10 strokes using pestle B (clearance 0.0010-0.0030"). Homogenate was centrifuged for 15 min at 12,000 x g. Supernatant was discarded and the pellet was resuspended in lysis buffer (6 mM Tris-maleate, cOmplete, pH 8.1) and incubated for 45 min. The suspension was centrifuged at 44,000 x g for 15 min. The pellet was discarded and the supernatant was centrifuged at 200,000 x g for 55 min. The pellet was gently dislodged with a Teflon-coated scraper and transferred to a 1.5 ml pre-chilled tube containing 200 to 400 µl storage buffer (0.32 M sucrose, 1 mM $NaHCO_3$, cOmplete, pH 7.2) for resuspension. A small aliquot (20 µl) was set aside for protein quantification. Dithiothreitol was added to the SV suspension to a final concentration of 1 mM and SVs aliquoted into pre-chilled O-ring conical tubes. Samples were stored either in liquid nitrogen for up to 1 yr [154] or snap frozen and stored for up to two weeks at -80°C. Aliquots of 200 µl from the homogenization and lysis steps from all preparations were used for protein quantification and Western blot analysis. Protein amounts were quantified using a Pierce BCA protein assay kit (Thermo Fisher Scientific).

For SV purification by a flotation gradient method [155, 156], neurons were homogenized as above in homogenization buffer (0.32 M sucrose, 10 mM Tris-HCl, cOmplete, pH 7.4). Homogenate was centrifuged for 10 min at 1,500 x g and supernantant was collected. The pellet was resuspended in homogenization buffer and centrifuged for 10 min at 1,500 x g. Supernatants were combined and centrifuged for 20 min at 20,000 x g. The pellet was resuspended in lysis buffer (5 mM Tris-HCl) for 45 min and then centrifuged for 20 min at 20,000 x g. The supernatant was collected and centrifuged for 45 min at 66,000 x g. The final pellet was resuspended in storage buffer (100 mM KCl, 10 mM NaCl, 1 mM $MgCl_2$, 10 mM K-phosphate buffer,

cOmplete, pH 7.4) containing 50% OptiPrep solution (v/v, 1:1 ratio, Sigma) and overlaid with storage buffer containing 40% OptiPrep solution. The resultant gradient was centrifuged for 3 h at 207,000 x g. SVs could not be observed in the OptiPrep layers. The protocol was successfully tested on brain tissue (data not shown).

3.3.4.2. Cortex

A single hemisphere cortex was isolated from one P18-P21 Wistar rat. Midbrain, cerebellum and olfactory bulb were removed and tissue was minced with a razor blade. SV isolation from cortex was performed as described above using differential centrifugation and buffer volumes described in previous work [154].

3.3.5. Trichloroacetic acid (TCA) precipitation

For each sample, the volume corresponding to 25 μg SV protein was brought to a final volume of 400 μl with water followed by addition of 100 μl of ice cold TCA (50% v/v) and vortexing. Samples were incubated on ice for 60 min and then centrifuged for 5 min at 4°C at 20,000 x g. Solvent was aspirated and replaced with 150 μl ice cold acetone. The pellet was washed twice by inverting the tube and the centrifugation step was repeated. The acetone was aspirated and samples were incubated at 37°C for 1 min to remove residual solvent. The pellet was resuspended in Laemmli buffer (40% v/v glycerol, 0.24 M Tris-HCl, 8% w/v sodium dodecyl sulfate (SDS), 0.04% w/v bromophenol blue, 5% v/v β-mercaptoethanol) to a final concentration of 0.5 to 1 μg/μl. The pellet was then incubated for 20 min at 37°C and for 5 min at 95°C followed by equilibration to RT and centrifugation (11,000 x g for 1 min). Samples were analyzed directly or after overnight storage at -20°C.

3.3.6. Western blot (WB)

WB analysis was performed using SDS-polyacrylamide gel electrophoresis as described previously [157]. Briefly, 12.5 μg precipitated protein was separated on 4-20% Mini-PROTEAN TGX gels (BioRad) in duplicate. One replicate gel was stained with 0.25% w/v Coomassie Brilliant Blue R-250 in staining solution (10% v/v glacial acetic acid and 45% v/v MeOH) for 3 h, then destained overnight in staining solution and recovered in distilled water for 1 h before imaging. The second replicate gel was electroblotted onto a polyvinylidene difluoride membrane. Membranes were blocked

with 5% w/v milk powder in Tris-buffered saline supplemented with 0.1% v/v Tween 20 for 1 h and incubated with primary antibodies against synaptophysin (dilution 1:5000, #101002, Synaptic Systems) and glutamate ionotropic receptor NMDA type subunit 1 (GluN1) (dilution 1:1000, #114011, Synaptic Systems) in blocking solution overnight at 4°C. Secondary antibody (goat anti-rabbit IgG(H+L)-horseradish peroxidase (HRP) conjugate or goat anti-mouse IgG(H+L)-HRP, dilution 1:10000, #170-6515, #170-6516, Biorad) was applied for 1 h at RT. Blots were developed with Clarity Western ECL Substrate (Biorad). Blots and gels were imaged with an Amersham 600RGB Imager (GE Healthcare). Total protein content from Coomassie-stained gels and levels of GluN1 and synaptophysin from blots were quantified in three biological replicates using Image Studio Lite software (LI-COR Biosciences). The level of GluN1 or synaptophysin per sample was normalized to total protein content of the respective duplicate lane.

3.3.7. ^{3}H-Glu uptake

Uptake assays were carried out as described previously [158, 159] with modifications. SV were thawed on ice for 30 min. Amounts corresponding to 10, 25 or 50 µg of total protein were suspended in 100 µl storage buffer. 80 µl of preincubation (PI) solution (final concentration: 20 mM HEPES, 90 mM K-gluconate, 4 mM KCl, 2 mM aspartate, 4 mM $MgSO_2$, pH 7.4 adjusted with Tris base) was added and the samples incubated on ice for 30 min. Samples were transferred to a heat block shaker and incubated for 10 min at 30°C and 500 RPM. 20 µl uptake solution (PI supplemented with 20 µM ^{3}H-Glu, Perkin-Elmer; specific activity 20 Ci/mmol, 1 mCi/ml) was added supplemented with either 2 mM ATP or water and incubated for 10 min at 30°C and 500 rpm. Reactions were stopped with 1 ml ice cold stop buffer (0.15 M KCl, 1 mM $MgCl_2$) and samples were transferred to ice. Samples were then filtered on Millipore HAWP filters (0.45 µm, 13 mm diameter) loaded with 5 mM K-glutamate. Sample tubes were washed twice and each filter was subsequently washed with a total volume of 20 ml of ice cold stop buffer. Filters were allowed to dry before adding them to scintillation vials with 10 ml of scintillation buffer (Carl Roth). Vials were shaken for at least 24 h and briefly vortexed before measurement. Radioactivity was measured in a Tri-Carb 2810 low activity liquid scintillation analyzer (PerkinElmer). Blank vials containing only the uptake solution were subtracted.

3.3.8. Antibody labeling and adsorption of SVs

Glass coverslips (1.5H, Marienfeld) were placed into a home-made holder and immersed for 4 h in Piranha solution (3:1 H_2SO_4:H_2O_2; prepared by slowly adding 150 ml of H_2SO_4 to 50 ml of 30% H_2O_2). The coverslips were washed 6 times in water and kept in water. On the day of imaging, coverslips were dried and placed in a plasma oven (Diener Electronic, 30 W setting) for 10 min. Imaging wells (5 mm diameter; [160]) were glued to the surface of the coverslip with optical adhesive (Norland) and dried under a UV lamp. Each well was coated with PLL (0.1% w/v) for 20 min, washed 3 times with water and allowed to dry. 0.1 to 10 μg of SVs were suspended in 50 μl uptake solution and allowed to adhere for 1 h at 4°C before imaging or antibody labeling. For staining, SVs were blocked with 5% w/v bovine serum albumin (BSA, Sigma) in phosphate buffered saline (PBS) for 30 min followed by primary antibody labeling against vesicular glutamate transporter 1 (VGluT1) (dilution 1:1000, #135303, Synaptic Systems) for 30 min. Samples were washed 3 times with 5% BSA in PBS and incubated with secondary antibody (Abberior STAR RED, dilution 1:1000, #41699, Sigma) for 20 min. Finally, SVs were washed 3 times with uptake solution and 30% OptiPrep in uptake solution was added to each well 10 min before imaging.

3.4.9. TIRF microscopy

An Olympus IX83 microscope equipped with cell^TIRF module and Olympus UApo oil immersion objective (100 x, NA 1.49) was employed to image SVs in TIRF illumination. Excitation wavelengths were 561 and 640 nm for tdimer2 and STAR RED, resp. Images were obtained using a quad line beam splitter emission filter (Chroma) and a EM-CCD camera (Hamamatsu). Samples were imaged for 20 frames at 1 Hz. Colocalization analysis was performed in Image J using the ComDet plugin (https://imagej.net/Spots_colocalization_(ComDet)). Projections of the median fluorescence intensities of each time lapse were used for analysis to minimize non-vesicle fluorescence. Colocalization was defined as the percentage of particles detected in the first channel that are also detected in the second channel. As an estimate for coincidental colocalization, one image was rotated 90° and reanalyzed (Fig. 3.2E). As a further control, images recorded from samples only treated with the secondary antibody were analyzed (Fig. 3.2E).

3.4. Results

3.4.1. SV isolation from cortical neuron culture

The goal of this work was to isolate SVs from cultured neurons that were transduced with lenti virus (Fig 3.1A). We chose cortical neurons because the cortex offers abundant starting material and because cortical neurons are a common *ex vivo* preparation and neuronal model system. As a first step, we estimated how much starting material will be required to isolate SVs for NT uptake and single SV imaging experiments. Between 20 and 60 μg of SV preparation (total SV protein amount) are typically required for a single NT uptake experiment, whereas smaller amounts (between 1 and 5 μg) are sufficient for WB analysis and single SV imaging [134, 135, 144, 154, 158]. In previous work, ~0.3 to 2 mg of SV protein amount were obtained from ~1 g of adult rodent brain tissue (wet weight) depending on the isolation and purification procedure [154, 161]. ~1 g of rat cortex contains ~30 to 50 x 10^6 mature neurons with active synapses [2, 162]. Accounting for variability in culture activity and viability, we decided that plating a total 120 x 10^6 neurons in four 15 cm dishes (30 x 10^6 neurons/dish) should provide sufficient SV material for uptake and imaging experiments in multiple conditions and with technical replicates.

For SV isolation, we adapted a differential centrifugation protocol developed by Kish and Ueda for brain tissue [154]. We harvested neurons into homogenization buffer and isolated SVs from lysed synaptosomes (Fig 3.1A). We minimized the amount of solution employed during tissue harvesting, lysis and SV storage to ensure high final SV concentrations while maintaining sample solubility and homogeneity. To demonstrate enrichment of SVs, we probed samples at each step of the procedure for synaptophysin, a marker for SV membranes, and for GluN1, a marker for intracellular and plasma membranes (Fig 3.1B). We found a robust enrichment of synaptophysin and a robust reduction of GluN1 that is comparable to that observed for intact cortex samples (Fig 3.1B) and for brain in literature [163, 164]. The final yield was 0.53 ± 0.10 mg total protein from one preparation consisting of four dishes. This result indicates that sufficient SV material for experiments can be obtained; however, the yield was somewhat lower than aforementioned estimate, which we attribute to differences in the activity and number of synapses in cultured neurons and intact cortex.

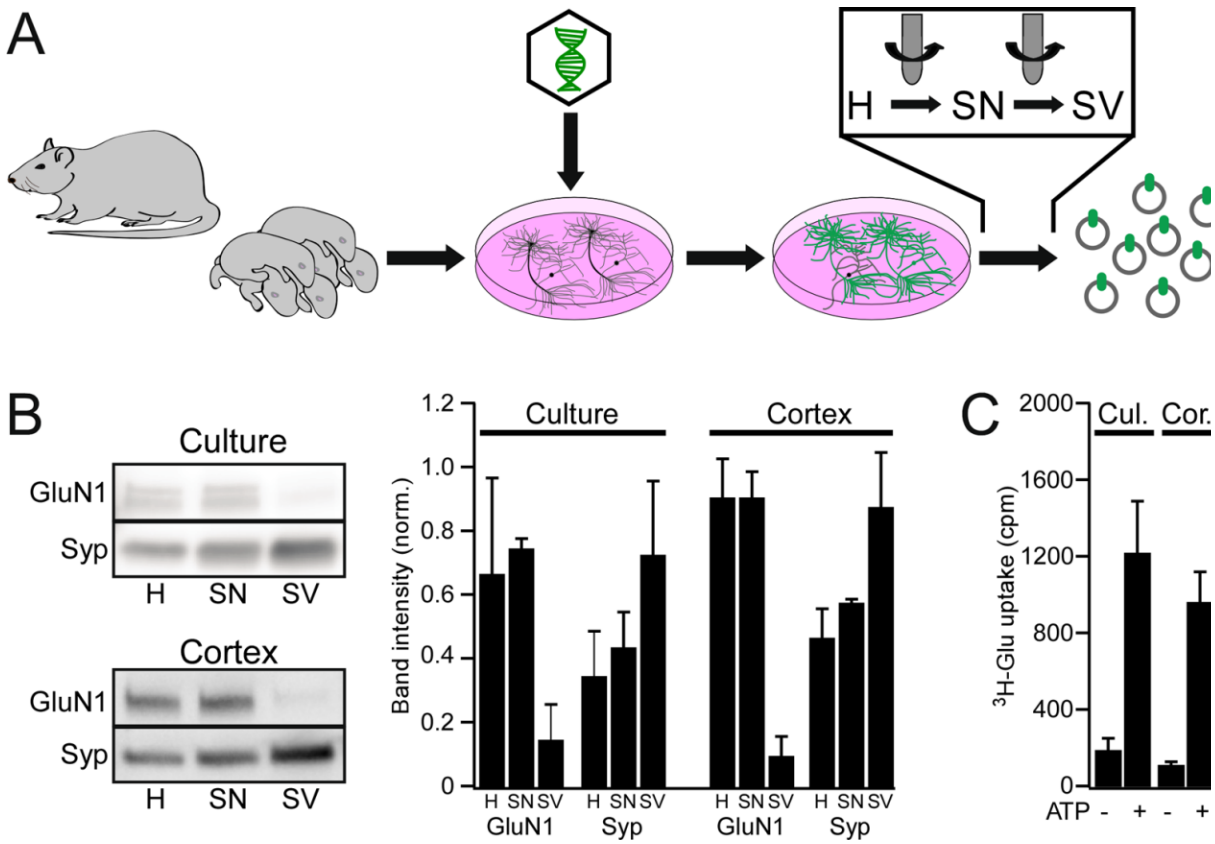

Fig 3.1 SV isolation procedure. (A) Cortical neurons are prepared from rat pups and transduced with lenti virus in culture. Cells are homogenized and SVs isolated from synaptosomes (SN). (B) WB analysis of a cell membrane marker (GluN1) and a SV marker (synaptophysin; syp) at each stage of the isolation procedure for cultured neurons and for cortex (H: homogenate; amount loaded: 12.5 μg in each lane). Band intensities are shown normalized to total protein (error bars denote S.D., n=3). (C) ^{3}H-Glu uptake for SVs isolated from cultured neurons and cortex (experiments were performed with 25 μg SV protein; error bars denote S.D., n=3).

SVs isolated using differential centrifugation from brain samples have in previous work been further purified using sedimentation velocity or sedimentation equilibrium centrifugation in density gradients. Although purification is not essential for functional experiments (see below and, e.g., [154, 158, 165]), we also tested if SVs isolated from cultured neurons are amenable to a gradient protocol that has been previously applied

to small SV sample amounts [147, 156]. However, we were not able to detect SV protein at the end of this protocol and focused on the robust differential centrifugation method.

3.4.2. ^{3}H-Glu uptake into SVs

To verify functionality of SVs isolated from cultured neurons, we evaluated ATP-dependent uptake of radiolabeled glutamate (^{3}H-Glu). We found that ^{3}H-Glu signals in the presence and absence of ATP were comparable for SVs isolated from cultured neurons and intact cortex (Fig 3.1C). Furthermore, the ATP-dependent signal increase for both preparations (e.g., for cultured neurons: 7.0 ± 0.4 fold, mean ± SD, n=3) was similar to that observed in previous work [154, 158]. These experiments were performed with 25 μg SV protein. We found that lower amounts did not permit reliable uptake measurements (10 μg: ATP-dependent increase was 3.1 ± 0.6 and 3.2 ± 1.3 fold, for culture and cortex, resp., n=3), whereas higher sample amounts resulted in improved ATP-dependent increase (50 μg: 13.2 ± 0.7 and 14.1 ± 1.1 fold for culture and cortex, resp., n=3 and n=5), as expected. These results demonstrate robust NT uptake function and allow us to propose a SV protein amount (25 μg) that permits reliable uptake measurements in a manual filtration system. At this amount, at least four uptake experiments with technical replicates can in our hands be performed with the material obtained from one four-dish preparation.

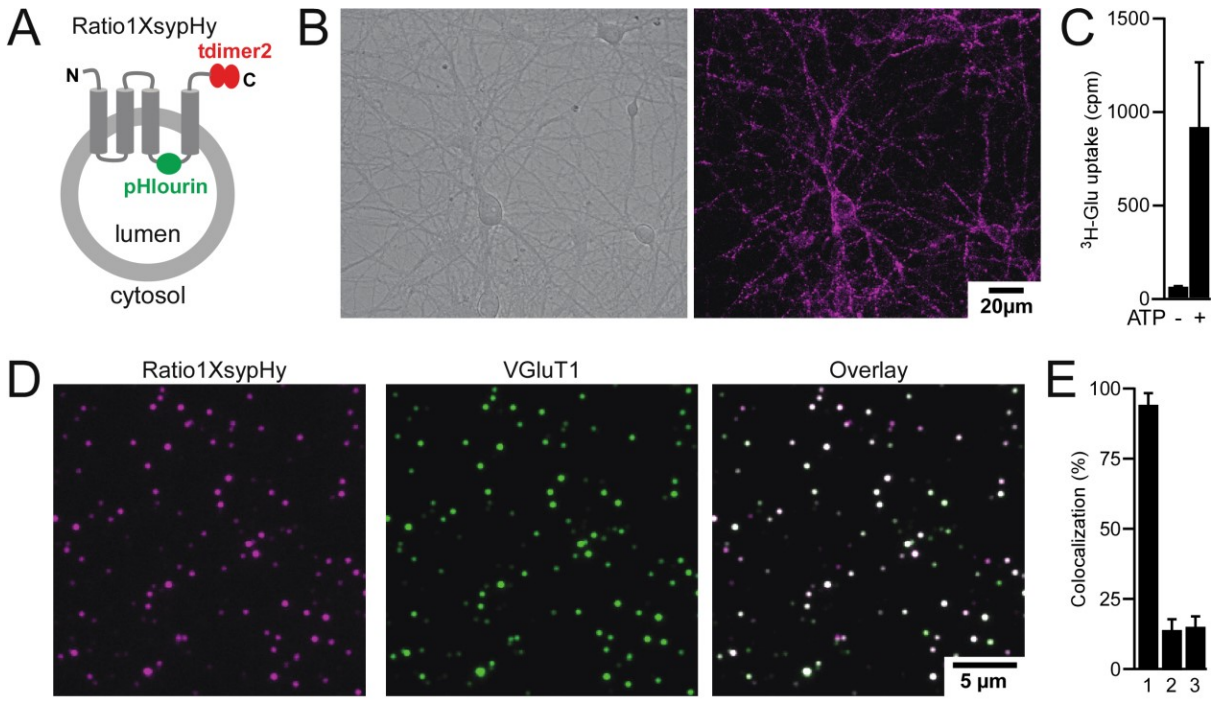

Fig 3.2. SVs from genetically modified neurons. (A) Ratio1XsypHy is synaptophysin modified with pHlourin on the luminal side and tdimer2 at the far CT. (B) Ratio1XsypHy expression in cortical culture (DIV18). Left: bright field. Right: tdimer2. (C) ^{3}H-Glu uptake into SVs isolated from transduced neurons (experiments were performed with 25 µg SV protein; error bars denote S.D., n=3). (D) TIRF microscopy of SVs expressing Ratio1XsypHy (tdimer2 signal) stained against VGluT1 (STAR RED signal). (E) Co-localization analysis of Ratio1Xsyphy with VGluT1. 1: Colocalization of VGluT1-positive particles with Ratio1XsypHy-positive particles. 2: Colocalization of VGluT1-positive particles with Ratio1XsypHy-positive particles after image rotation. 3: Colocalization of Ratio1XsypHy-positive particles with VGluT1-positive particles in the absence of primary antibody. Error bars denote S.D., n=4-5.

3.4.3. SVs from genetically engineered neurons

To test the overall procedure, we went on to characterize SVs isolated from cortical neurons that were virally transduced to express an exogenous SV-localized protein. Fluorescently-tagged synaptophysins are commonly employed as genetically

encoded sensors for SV trafficking and fusion [153, 166, 167]. Ratio1XsypHy [138] is a dual-color synaptophysin-based sensor that contains pHlourin, a pH sensitive variant of GFP in the luminal domain between the transmembrane helix 3 and 4, and tdimer2 [168], a red fluorescent protein tandem dimer at the cytosolic CT (Fig 3.2A). Ratio1XsypHy previously served to visualize SV trafficking (using the tdimer2 signal) and fusion (using increased pHluorin fluorescence upon SV deacidification). We first validated Ratio1XsypHy expression in cortical neurons after transduction with a lenti virus and under the control of the human synapsin promoter. We observed a punctate expression pattern that is typical for SVs and synaptophysin-based sensors in cultured neurons (Fig 3.2B) [169]. Next, we isolated SVs from the transduced neurons, verified ATP-dependent ^{3}H-Glu uptake (Fig 3.2C), and established conditions for single vesicle imaging in TIRF microscopy. We chose TIRF microscopy due to its ability to sensitively and selectively visualize particles adhered to a surface. We found that adsorption of 100 ng of SV protein in 5 mm imaging wells permitted visualization of individual Ratio1XsypHy-positive SVs (Fig 3.2D, left), whereas adsorption of 1 or 10 μg produced comparable images that did not permit detection of single fluorescent particles (Fig 3.3). To quantify the efficiency of SV modification, we stained SVs against VGluT1, a vesicular marker for glutamatergic neurons [170] (Fig 3.2D, right). We observed comparable numbers of fluorescent particles in the Ratio1XsypHy channel and in the VGluT1 channel (466 ± 70 and 423 ± 28, resp.; mean ± SD, n=5). We further found that fluorescent signals from VGluT1 showed high colocalization with signals from Ratio1XsypHy, and vice versa, whereas both a confidence test (rotation of the Ratio1XsypHy image by 90°) and negative controls (secondary antibody only) exhibited poor colocalization (Fig 3.2E). The level of colocalization demonstrates robust viral delivery of a gene that encodes a SV-targeted protein to the cultured neurons and the overall efficiency of the method.

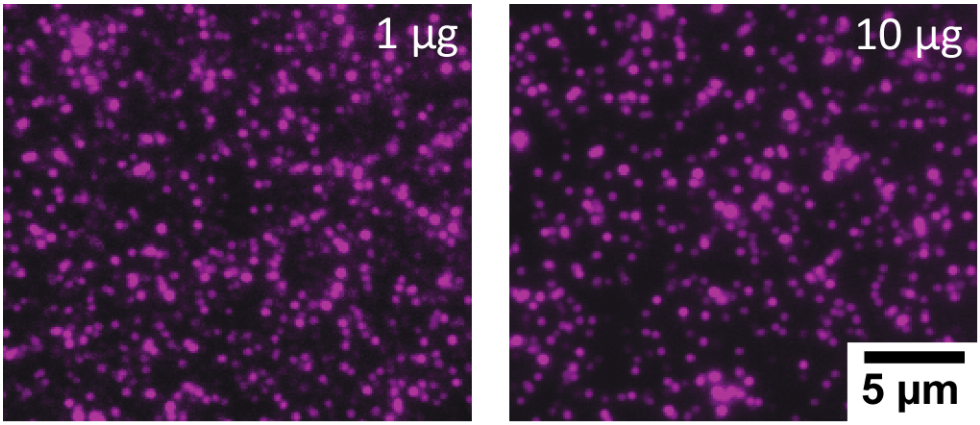

Fig. 3.3 TIRF microscopy of SVs expressing Ratio1XsypHy (tdimer2 signal) adsorbed at higher SV protein amounts.

3.5. Discussion

Experiments with isolated SVs from genetically engineered neurons have in the past generally relied on the availability of transgenic animals. This approach is constrained by cost, time and a limited ability to manipulate some of the key proteins involved in SV function because of developmental defects, lethality and compensation [149-152]. Collectively, these limitations may explain the relatively small number of studies that describe the structure or function of SVs after genetic modification [144, 147-149] despite continued strong interest in SV biology.

Here, we demonstrate the isolation and characterization of SVs from genetically engineered cortical neuron cultures. Our results show that 120 x 10^6 cortical neurons processed by differential centrifugation provide sufficient SVs for functional experiments. SVs obtained from the cultured neurons showed comparable enrichment and reduction of marker proteins and ATP-dependent activity to reference preparations from cortex. We identified the lowest amounts for which reliable imaging and uptake measurements can be performed in our hands to be 100 ng and 25 µg, respectively. These numbers indicate that multiple experiments with controls and technical replicates can be conducted using the material obtained from one preparation. We also demonstrated that manipulation of SVs in cortical neurons was efficient. ~95% of the fluorescent particles that stained for a marker for SVs of glutamatergic neurons, which comprise the main neuron type in the cortex [171, 172],

also expressed the genetically introduced synaptophysin marker. In two previous studies, SVs were isolated from cultured neurons, which in one case were transduced with a virus [147, 153]. These studies did not disclose the amount of starting material, did not report SV function and employed a gradient-based method that could not be successfully applied to our cultured neuron samples.

We anticipate that the ability to isolate functional SVs from genetically engineered cultured neurons will enable new combined *in vitro* and *in situ* studies. Isolated SVs are required as a starting material for a number of methods. These include quantitative, i.e. calibrated to vesicle number [133], ensemble biochemical and bioenergetics analyses (e.g. by WB or mass spectrometry) as well as single SV analyses (e.g. by advanced microscopy or fluorescence-activated sorting). These techniques can now be more readily applied to preparations from genetically engineered neurons, in which the levels of specific proteins are increased or decreased or in which proteins are modified with mutations or larger domain deletions/insertions. Chemically transfected cultured cell lines, e.g. rat pheochromocytoma cells, have in the past enabled the identification and characterization of SV proteins through the isolation of SV-like microvesicles [173, 174]. These studies highlight further possible applications of genetically engineered neuron cultures, which are physiologically representative and can be obtained from a specific brain region or enriched in a specific neuron type. Overall, these studies will be facilitated by the growing availability and capability of gene delivery techniques, in particular engineered viruses, which can be tuned to selectively transduce specific cell populations with low toxicity or harbor cell-type specific promoters.

A number of neurochemical properties and neurophysiological processes come to mind that may be studied by combining SV isolation, SV *in situ* analysis and genetic modification. These include revealing molecular determinants of different vesicle pools and their response to protein content perturbations, compensation in SV protein composition and variability between SVs, or the impact of post-translational modifications on SV protein function. Furthermore, the ability to introduce mutations may enable revealing molecular structure-function relationships of the vesicular proteins and their cellular binding partners that contribute to synaptic communication processes. In general, drawing parallels between SV content and function may

contribute to the identification of new drug targets and an understanding of existing and new disease models.

3.6 Conclusions

We demonstrate the isolation of SVs from genetically engineered cultured neurons. The function of the isolated SVs recapitulated the function of SVs obtained from intact cortical tissue. Genetic modification of SVs was efficient with high colocalization of an endogenous and an exogenous SV marker protein. Our work shows that SVs from genetically engineered neurons are accessible without the need for transgenic animals, and we anticipate that it will lead to new studies that draw parallels from *in vitro* and *in situ* analysis of SV content, structure and function.

Chapter 4: Towards Synthetic Neurotransmission

I would like to thank Ingrid Chamma (Institute for Interdisciplinary Neuroscience, University of Bordeaux) for assistance with release assay imaging and Olivier Thoumine (Institute for Interdisciplinary Neuroscience, University of Bordeaux) for the use of his lab and equipment. This chapter contains unpublished data.

4.1. Outlook

In the previous chapters, I have shown that a Met-gated ion channel can be engineered for efficient gating and expression in mammalian cells and that cultured neurons can be transduced with lenti-virus to serve as a rapid test bed for assessing the function of SV proteins. Open questions towards the realization of synthetic neurotransmission (SNT) are, by what mechanism will Met be imported into the presynaptic neuron and further into SVs to achieve the goal of Met co-release, as well as, what experimental systems are in place to test SNT.

It is well known that plasma membrane (PM) transporters of the SLC family, such as the L-type amino acid transporter type 1 (LAT1) are expressed in neurons [175-178]. LAT1 is a Na^+-independent high-affinity transporter of large neutral amino acids, one of the primary transporters of Met [179, 180], and a necessary component for supplying neurons with Met for metabolic purposes [181]. LAT1 exhibits concentration based competitive transport of its substrates and elevation of Met is preferentially transported across the BBB and PMs [182] by monopolizing LAT1 as is the case for other known substrates, such as phenylalanine [179, 180, 183, 184]. To validate LAT1 expression and Met-uptake, I performed preliminary experiments in dissociated cerebellar granule cells (CGCs) and hippocampal neuronal culture (HNC) (Fig 4.1A). I found that immunolabeling against LAT1 showed high levels of expression both in CGCs and hippocampal neurons. I also found that Met-uptake in dissociate hippocampal culture is efficient (Fig 4.1B) and can be partially blocked with 2-aminobicyclo[2.2.1]heptane-2-carboxylic acid (BCH), a specific inhibitor of L-type amino acid transporters. While there was a significant reduction in ^{3}H-Met uptake with BCH, it remains unclear here to what extent other transport systems contribute to Met PM uptake. The sodium-coupled neutral amino acid transporters, like SNAT2 [185] are also expressed in neurons [186, 187] and catalyze unidirectional Met PM transport [187]. Immunostaining for SNAT2 in HNC and CGCs showed undetectable expression levels (data not shown); however, this may be more a problem of antibody efficiency than absence of protein, as SNAT2 has been shown to express in neurons elsewhere [186]. Therefore it is likely that the majority of Met uptake in neurons is a combination of SNAT2 and LAT1. This taken with LAT1 Met preference in a concentration dependent manner [179] shows that there are most likely sufficient endogenous systems in place for Met PM uptake and thus suit the purposes required here. A more

intensive pharmacological experimental paradigm (e.g. increasing the range of Met transporter blockers) in a pure neuronal culture (e.g. Banker's culture) [188] would be required to determine specific concentrations of Met uptake in neurons.

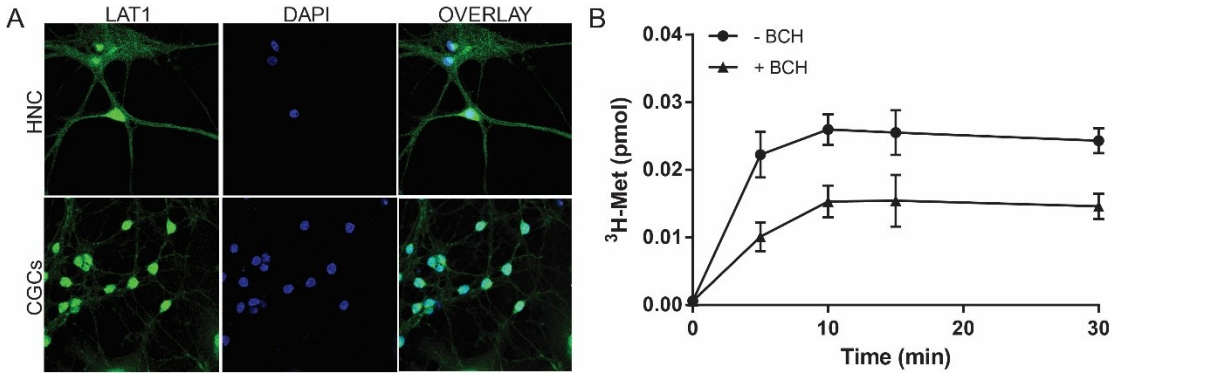

Fig 4.1. LAT1 facilitates Met uptake in neurons. (A) Immunolabeling against LAT1 (rabbit anti-LAT1, 1:200 dilution, Santa Cruz biotechnologies #F0414, secondary antibody 1:500 dilution, 488 AlexaFluor™ goat-anti-rabbit, antibody labeling was performed as described in chapter 2). (B) Radiolabeled Met uptake in HNC as described previously [189] with modifications. Briefly, cells were cultured as in chapter 2, washed once with warmed PBS and incubated in sodium buffer (140 mM NaCl, 5 mM KCl, 5.6 mM D-glucose, 0.9 mM CaCl2, 1 mM MgCl2, and 10 mM HEPES, pH 7.3) containing ^{3}H-Met (supplemented with cold Met at a ratio of 1:1000) with 1 mM BCH (diamonds) or without (circles). Uptake was stopped by the addition of 3x wash with ice-cold sodium buffer and lysed in 1M NaOH. Lysate was diluted in scintillation buffer and tritium counts were read (see chapter 3). Uptake experiments were performed at 37°C. Error bars denote ± SD., n = 2, for each n conditions were run in duplicate.

Whereas PM uptake of Met is enabled by members of a transporter families that are expressed ubiquitously, such transport systems do not exist in SVs.

Neurotransmitter (NT) identity is a feature of all neurons because it delineates the type of information conveyed. While the general assumption is that classes of neurons release a singular NT, exceptions continue to amass. The concept of co-release has gained recent traction with the discovery dual NT species released from

neuronal types previously thought to be NT specific [190]. It has been previously reported that SVs have the ability to load multiple NT species [190-192], and there is evidence that a singular SV contains dual transporters, as in the case of VGluT2 and VMaT2 [193, 194]. Variants of monoamines, as in the case of false fluorescence neurotransmitters [195] and non-selective uptake of stereoisomers of glutamate [53] have been shown to package into SVs. In the case of Met, which share the same zero-charge as Dopa and GABA [196], taken with the above, it is reasonable to hypothesize dual SV filling of Met through a synthetic VT may be well tolerated.

I thus identified candidate proteins for the role of a vesicular Met-importer (Table 4.1). These transporters are primarily microbial exporters, part of the Amino acid-Polyamine-organoCation superfamily [197] that thus may transport Met into SVs. Two of the transporters have been characterized in their native system and were shown to be powered by proton gradients (and thus harness the natural import driving force in SV NT packaging) [198, 199]. One candidate is a high affinity Met permease from yeast (see Table 4.1) that is solely concentration dependent uptake. These candidate transporters carry the added advantage in they rely on them as single genes, unlike the high affinity Met transport systems found in many prokaryotic species which relies on a multiple gene expression for functionality, such as *brnFE* genes in a *C. glutamicum* strain [200] or the *E. coli* MetD system [201]. In addition to and in line with the above, it is important to note that, at least for glutamatergic synapses, which are a first choice for this method, I do not expect that the expression of additional transporters in SVs will alter loading of the endogenous neurotransmitter as it was previously shown that more transporter means more Glu, i.e. H^+ gradient are not exhausted [202]. To target these non-mammalian proteins to SVs, I have designed a repurposed syn gene. One set of the candidate transporters were directly inserted between the 3rd and 4th helices of the Ratio1Xsyphy construct used in chapter 3, the other set of transporter candidates an additional helices was inserted after the transporter gene, for correct transporter orientation in the SV membrane (Fig 4.2A). This design has proven to be an effective targeting strategy for prokaryotic proteins targeted to mammalian SVs [57]. I refer to these constructs as vesicular methionine transporters (VMetTs). For VMetT candidate 1 (VMetT1) delivered into hippocampal neurons, I was able to show that trafficking is directed to pre-synaptic structures with

microsopy (Fig 4.2 B,C) and a stimulated release assay revealed functional fusion events (Fig 4.2 D)

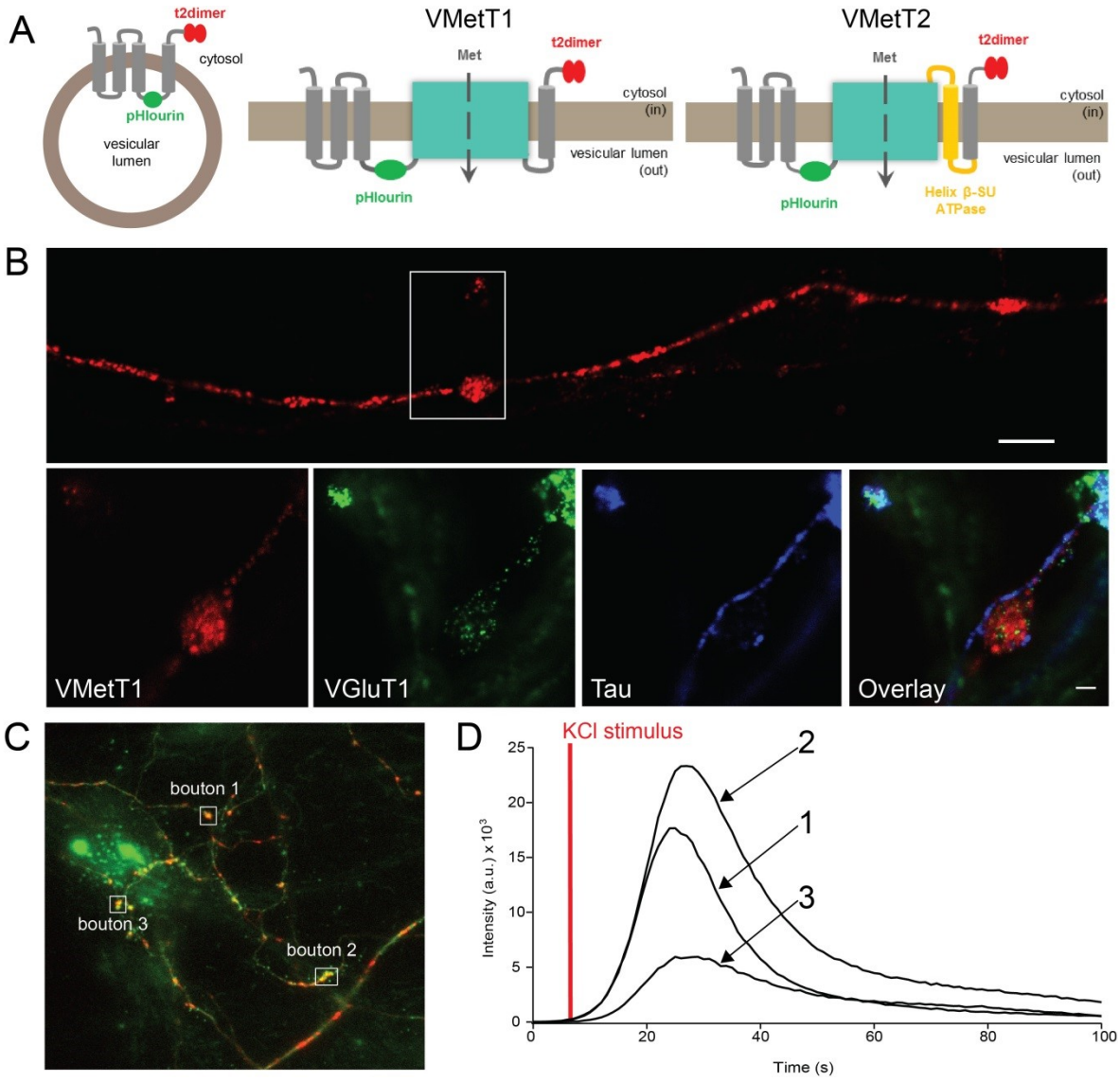

Fig 4.2. Targeting prokaryotic methionine transporters to SVs (A) Design of targeting strategy. (B) Hippocampal axon in dissociated culture expressing VMetT1 (B, Upper panel confocal) (scale bar denotes 10 µm). STED images of VMetT1 (B, left), VGluT1 (center left), Tau (center right) overlay image (far right) shows localization within an axonal bouton (scale bars denote 1 µm). (C,D) High potassium stimulation reveals release events. Histogram of fluorescence intensity (green channel) for three identified boutons expressing VMetT1.

A system such as SNT, designed to synthetically connect two distinct sub-cellular populations, must first be broken down to its individual parts and characterized separately. The final step in proof of concept is therefore bringing these components back together in a system that can easily identify successful SNT. An experimental system that fits these requirements well is co-culture, culturing two populations of cells that distinctly express proteins of interest [79]. Creating simplified PSDs by expressing base unit proteins, like neuroligins and membrane-associated guanylate kinases in cell lines, create faux synapses when cultured at defined time points with a wide variety of neuronal types and can be used extract information about protein dynamics in synaptic interactions [203, 204]. I established this system to show that channel activation can be observed in a synapse specific manner (Fig 4.3).

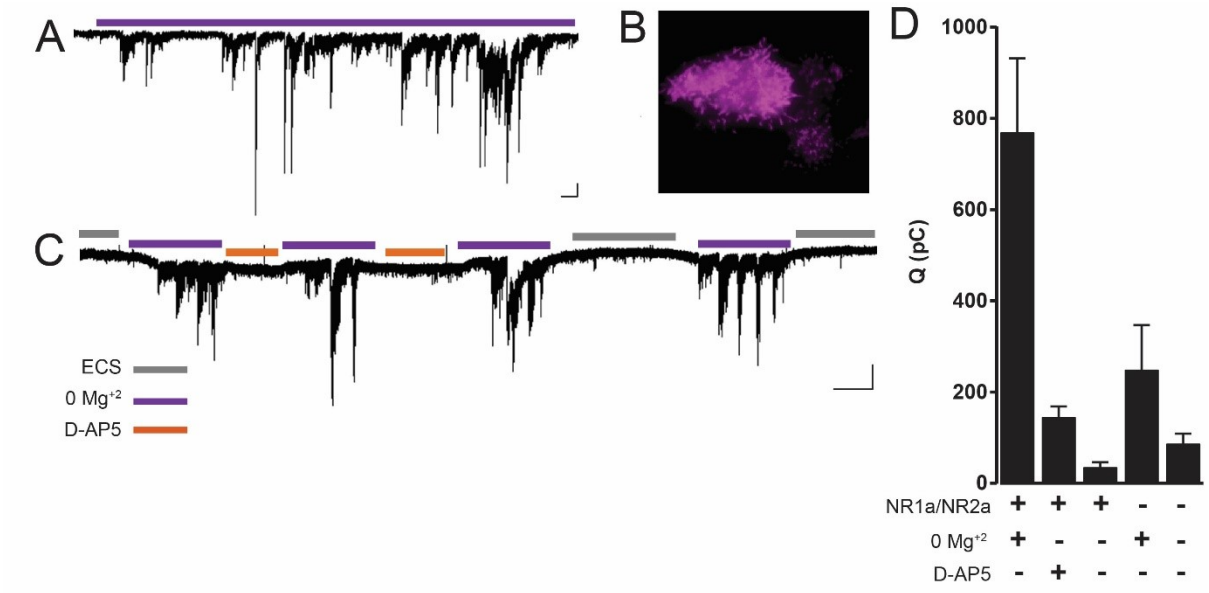

Fig 4.3. Neuron-HEK 293 co-culture (A) Representative paroxysmal currents from CGCs in whole cell gap free mode with application of Mg^{+2} free bath solution. (B) HEK 293 cell expressing neuroligin-1 CT tagged with eGFP in TIRF (100x). (C) Representative paroxysmal currents in HEK 293 cells expressing neuroligin1, PSD-95, and NMDAR subunits 1-1a and 2A, transfections were carried out as in chapter 2. Currents were elicited with application of Mg^{+2} free bath solution and could be eliminated with D-AP5 (specific NMDAR inhibitor) or inclusion of Mg^{+2} in the bath solution. (D) Comparison of total charge elicited from faux synapse in HEK 293 cells

in gap free whole cell patch clamp under various conditions. All experimental procedures were carried out as previously describe [203]. Error bars denote ± SD., scale bars represent 0.1 nA and 10 s.

Viral targeting of VMetTs to a dissociated neuronal culture (chapter 3) in conjunction with a cell line expressing iMetR tagged PSD-95 complexing variants (chapter 2) to create a faux synapse would allow electrophysiological or calcium imaging experiments to be performed with ease (e.g. no additional blockers to isolate iMetR current) and provide valuable insight into Met-iMetR dynamics across synapses in a SNT fashion.

4.2. Discussion

Biological methods created to study components of neuronal communication by targeting one neuronal type en masse have in recent years aided in the dissection of genetically define circuits. While much of this ground is covered by the advent of optogenetics and chemogenetics there is still much left to be desired. As with any tool, understanding the limitations or possible negative consequences that may arise from the implementation or use of that tool is critical information and worth addressing.

Readily used chemogenetic tools like DREADD (metabotropic) [205] and PSEM/PSAMs (ionotropic) [50] have faced application based challenges. DREADDs have come into orthogonality conflict with the preferred designer ligand CNO, which has been recently shown to be BBB impermeable [206], rather its metabolite, clozapine, a well-known anti-psychotic, readily crosses the BBB instead. This shift in designer ligand, while a much more potent activator of DREADDs, may cause un-specific activation of native receptors, which may be masked by larger synthetic signals inside the region of interest or unobserved, due to activation outside of the observed region of interest. Unlike the case of CNO-clozapine, Met is readily taken up by the BBB and while metabolites of Met like homocysteine, have been shown to cause toxicity at only very high levels [207, 208], the Met metabolic cycle important for homeostatic regulation of homocysteine levels is an effective endogenous counter-measure, and in fact acute increases in Met have been shown to carry neuroprotective properties (see chapter 2). In the case of PSEM/PSAM, prolonged durations of PSEMs for excitatory overrides due to inefficient ligand clearing may lead to excitotoxicity.

Unlike the PSEMs, housekeeping of elevated levels of Met may overcome undesired excitotoxicity. More globally, a major challenge for any biological method is controlling the amount of non-native protein levels while still producing the desired outcome. Overexpression of any exogenous protein may compete for space with native proteins [209] or change intrinsic membrane properties [210] both of which intrinsically alter the focused behavior intended to modulate; this can be countered by decreasing the level of introduced protein by integrative virus and promoter strength *ex vivo* and genetic models *in vivo*.

To conclude, I have introduced methods and components towards realizing a SNT system. Our aim with SNT is to provide a method that allows researchers the ability to manipulate the analog signals of a predefined post-synaptic target by designated pre-synaptic digital output, using the power of the natural signaling machine of the pre-synapse. This is of great value for three major reasons. The first being, all divergent and convergent information coming from upstream and/or collateral targets is preserved. Second, targeting a specific synaptic type (glutamatergic versus GABAergic) will allow subcellular dissection of the importance of that synaptic pair on the analog computation of the post-synaptic target and third, it is well know that the breakdown of communication between neuronal types that lead to severe neurological disorders (like Parkinson's or Alzheimer's) is not binary or immediate, rather it is a slow degenerative process and a system which one could modulate subcellular connectivity would be of great value in understanding the onset of neurological disorders. Off target effects can be difficult to side step or eliminate completely, especially if they are not paired with electrical observation or simply too subtle at first to be observed yet amplify overtime with repeated exposure of light or ligand. One other advantage of a SNT system is that any gain of function can be pin pointed back to the original source of modulated synapses. In order to understand in greater detail the causal link between the analog to digital conversion in cell-cell communication and behavior in health and disease, the concerted application of current tools such as genetic manipulation (e.g. transgenic animal models such as MADM [211]), electrical monitoring (e.g. implantable electrodes), and high resolution imaging (e.g. endoscopic and multi-photon imaging [212]) *in vivo* with biological systems, like SNT, will generate new data sets and will bring new insights to the causal relationships in the mammalian brain.

Table 4.1 Candidate Met Exporters

Name	Gene	Function	Driving force	Organism	Uniprot ID/ACCESSION	Source	Predicted helcies
VMetT1	Yeas	Met/Leu exporter	electrochemical gradient	*Escherichia coli*	P76249	[198]	6
VMetT2	Yjeh	Met exporter	electrochemical gradient	*Escherichia coli*	P39277	[199]	11
VMetT3	Yeas Homolog 1	unknown	unknown	*Chromobacterium violaceum*	WP_011137350.1	n/a	n/a
VMetT4	Yjeh Homolog 1	unknown	unknown	*Chromobacterium violaceum*	WP_011136979.1	n/a	n/a
VMetT5	Yeas Homolog 2	unknown	unknown	*Desulfovibrio magneticus*	WP_006921580.1	n/a	n/a
VMetT6	Yjeh Homolog	unknown	unknown	*Vibrio harveyi*	WP_017188716.1	n/a	n/a
VMetT7	MUP1	Met permease	concentration gradient	*Yeast*	P50276	[213]	10

References

1. Internetlivestats. *Total number of websites*. Available from: http://www.internetlivestats.com/total-number-of-websites.
2. Herculano-Houzel, S., et al., *Mammalian Brains Are Made of These: A Dataset of the Numbers and Densities of Neuronal and Nonneuronal Cells in the Brain of Glires, Primates, Scandentia, Eulipotyphlans, Afrotherians and Artiodactyls, and Their Relationship with Body Mass.* Brain Behav Evol, 2015. **86**(3-4): p. 145-63.
3. Drachman, D.A., *Do we have brain to spare?* Neurology, 2005. **64**(12): p. 2004-5.
4. Friston, K.J., *Functional and effective connectivity: a review.* Brain Connect, 2011. **1**(1): p. 13-36.
5. Negyessy, L., et al., *Convergence and divergence are mostly reciprocated properties of the connections in the network of cortical areas.* Proc Biol Sci, 2008. **275**(1649): p. 2403-10.
6. Mochizuki, Y. and S. Shinomoto, *Analog and digital codes in the brain.* Phys Rev E Stat Nonlin Soft Matter Phys, 2014. **89**(2): p. 022705.
7. Euler, T., et al., *Retinal bipolar cells: elementary building blocks of vision.* Nat Rev Neurosci, 2014. **15**(8): p. 507-19.
8. Alle, H. and J.R. Geiger, *Analog signalling in mammalian cortical axons.* Curr Opin Neurobiol, 2008. **18**(3): p. 314-20.
9. Yu, J., H. Qian, and J.H. Wang, *Upregulation of transmitter release probability improves a conversion of synaptic analogue signals into neuronal digital spikes.* Mol Brain, 2012. **5**: p. 26.
10. Bas-Orth, C. and H. Bading, *The divergence-convergence model of acquired neuroprotection.* Mech Dev, 2013. **130**(6-8): p. 396-401.
11. Twine, N.A., et al., *Sequencing of hippocampal and cerebellar transcriptomes provides new insights into the complexity of gene regulation in the human brain.* Neurosci Lett, 2013. **541**: p. 263-8.
12. Telese, F., et al., *"Seq-ing" insights into the epigenetics of neuronal gene regulation.* Neuron, 2013. **77**(4): p. 606-23.
13. Goff, L.A., et al., *Spatiotemporal expression and transcriptional perturbations by long noncoding RNAs in the mouse brain.* Proc Natl Acad Sci U S A, 2015. **112**(22): p. 6855-62.
14. Jackson, A.C. and R.A. Nicoll, *The expanding social network of ionotropic glutamate receptors: TARPs and other transmembrane auxiliary subunits.* Neuron, 2011. **70**(2): p. 178-99.
15. Khazen, G., et al., *Combinatorial expression rules of ion channel genes in juvenile rat (Rattus norvegicus) neocortical neurons.* PLoS One, 2012. **7**(4): p. e34786.
16. Jeanne, J.M. and R.I. Wilson, *Convergence, Divergence, and Reconvergence in a Feedforward Network Improves Neural Speed and Accuracy.* Neuron, 2015. **88**(5): p. 1014-1026.

17. Froula, J.M., et al., *alpha-Synuclein fibril-induced paradoxical structural and functional defects in hippocampal neurons.* Acta Neuropathol Commun, 2018. **6**(1): p. 35.
18. Wu, T., M. Hallett, and P. Chan, *Motor automaticity in Parkinson's disease.* Neurobiol Dis, 2015. **82**: p. 226-234.
19. Bates, G.P., et al., *Huntington disease.* Nat Rev Dis Primers, 2015. **1**: p. 15005.
20. Malejko, K., et al., *Prodromal Huntington disease as a model for functional compensation of early neurodegeneration.* PLoS One, 2014. **9**(12): p. e114569.
21. Reiner, A., et al., *Striatal parvalbuminergic neurons are lost in Huntington's disease: implications for dystonia.* Mov Disord, 2013. **28**(12): p. 1691-9.
22. Soloveva, M.V., et al., *A critical review of brain and cognitive reserve in Huntington's disease.* Neurosci Biobehav Rev, 2018. **88**: p. 155-169.
23. Glazebrook, J.F. and R. Wallace, *Pathologies in functional connectivity, feedback control and robustness: a global workspace perspective on autism spectrum disorders.* Cogn Process, 2015. **16**(1): p. 1-16.
24. Dennis, E.L. and P.M. Thompson, *Functional brain connectivity using fMRI in aging and Alzheimer's disease.* Neuropsychol Rev, 2014. **24**(1): p. 49-62.
25. Dai, Z., et al., *Identifying and Mapping Connectivity Patterns of Brain Network Hubs in Alzheimer's Disease.* Cereb Cortex, 2015. **25**(10): p. 3723-42.
26. Ramani, R., *Connectivity.* Curr Opin Anaesthesiol, 2015. **28**(5): p. 498-504.
27. Livet, J., et al., *Transgenic strategies for combinatorial expression of fluorescent proteins in the nervous system.* Nature, 2007. **450**(7166): p. 56-62.
28. Weissman, T.A. and Y.A. Pan, *Brainbow: new resources and emerging biological applications for multicolor genetic labeling and analysis.* Genetics, 2015. **199**(2): p. 293-306.
29. Navlakha, S., et al., *A high-throughput framework to detect synapses in electron microscopy images.* Bioinformatics, 2013. **29**(13): p. i9-17.
30. Beier, K. and C. Cepko, *Viral tracing of genetically defined neural circuitry.* J Vis Exp, 2012(68).
31. Wouterlood, F.G., et al., *A fourth generation of neuroanatomical tracing techniques: exploiting the offspring of genetic engineering.* J Neurosci Methods, 2014. **235**: p. 331-48.
32. Erdmann, J., *Brain projects plot neural connections.* Chem Biol, 2013. **20**(5): p. 627-8.
33. Deisseroth, K., *Optogenetics: 10 years of microbial opsins in neuroscience.* Nat Neurosci, 2015. **18**(9): p. 1213-25.
34. Zhang, K. and B. Cui, *Optogenetic control of intracellular signaling pathways.* Trends Biotechnol, 2015. **33**(2): p. 92-100.
35. English, J.G. and B.L. Roth, *Chemogenetics-A Transformational and Translational Platform.* JAMA Neurol, 2015. **72**(11): p. 1361-6.
36. Sternson, S.M. and B.L. Roth, *Chemogenetic tools to interrogate brain functions.* Annu Rev Neurosci, 2014. **37**: p. 387-407.
37. Cajal, S.R., *Conexion general de los elementos nerviosos.* Med Pract, 1889. **2**: p. 341-346.
38. Foster, M., *A textbook in physiology. Part three: The central nervous system*. 7th edn. ed1897, London: Macmillan.
39. Elliott, T.R., *On the action of adrenaline.* J Physiol Lond, 1904. **31**: p. xx-xxi.
40. Langley, J.N., *On the reaction of cells and of nerve-endings to certain poisons, chiefly as regards the reaction of striated muscle to nicotine and to curari.* J Physiol, 1905. **33**(4-5): p. 374-413.

41. Loewi, O. and E. Navratil, *Über hormonale Übertragbarkeit der Herznervenwirkung.* Pflügers Arch, 1926. **214**(678-688).
42. Noda, M., et al., *Primary structure of alpha-subunit precursor of Torpedo californica acetylcholine receptor deduced from cDNA sequence.* Nature, 1982. **299**(5886): p. 793-7.
43. Tansey, E.M., *Henry Dale and the discovery of acetylcholine.* C R Biol, 2006. **329**(5-6): p. 419-25.
44. Gothert, M., *Serotonin discovery and stepwise disclosure of 5-HT receptor complexity over four decades. Part I. General background and discovery of serotonin as a basis for 5-HT receptor identification.* Pharmacol Rep, 2013. **65**(4): p. 771-86.
45. Takagaki, G., *The dawn of excitatory amino acid research in Japan. The pioneering work by Professor Takashi Hayashi.* Neurochem Int, 1996. **29**(3): p. 225-9.
46. Valenstein, E.S., *The discovery of chemical neurotransmitters.* Brain Cogn, 2002. **49**(1): p. 73-95.
47. Carlsson, A., *Thirty years of dopamine research.* Adv Neurol, 1993. **60**: p. 1-10.
48. Nistri, A. and A. Constanti, *Pharmacological characterization of different types of GABA and glutamate receptors in vertebrates and invertebrates.* Prog Neurobiol, 1979. **13**(2): p. 117-235.
49. Janovjak, H., et al., *A light-gated, potassium-selective glutamate receptor for the optical inhibition of neuronal firing.* Nat Neurosci, 2010. **13**(8): p. 1027-32.
50. Magnus, C.J., et al., *Chemical and genetic engineering of selective ion channel-ligand interactions.* Science, 2011. **333**(6047): p. 1292-6.
51. Coward, P., et al., *Controlling signaling with a specifically designed Gi-coupled receptor.* Proc Natl Acad Sci U S A, 1998. **95**(1): p. 352-7.
52. Armbruster, B.N., et al., *Evolving the lock to fit the key to create a family of G protein-coupled receptors potently activated by an inert ligand.* Proc Natl Acad Sci U S A, 2007. **104**(12): p. 5163-8.
53. Pan, Z.Z., G. Tong, and C.E. Jahr, *A false transmitter at excitatory synapses.* Neuron, 1993. **11**(1): p. 85-91.
54. Gubernator, N.G., et al., *Fluorescent false neurotransmitters visualize dopamine release from individual presynaptic terminals.* Science, 2009. **324**(5933): p. 1441-4.
55. Chen, G.Q., et al., *Functional characterization of a potassium-selective prokaryotic glutamate receptor.* Nature, 1999. **402**(6763): p. 817-21.
56. Janovjak, H., G. Sandoz, and E.Y. Isacoff, *A modern ionotropic glutamate receptor with a K(+) selectivity signature sequence.* Nat Commun, 2011. **2**: p. 232.
57. Rost, B.R., et al., *Optogenetic acidification of synaptic vesicles and lysosomes.* Nat Neurosci, 2015. **18**(12): p. 1845-1852.
58. Green, K.A., S.J. Harris, and G.A. Cottrell, *Dopamine directly activates a ligand-gated channel in snail neurones.* Pflügers Arch, 1996. **431**(4): p. 639-44.
59. Mueller, K.L., et al., *The receptors and coding logic for bitter taste.* Nature, 2005. **434**(7030): p. 225-9.
60. Zhao, G.Q., et al., *The receptors for mammalian sweet and umami taste.* Cell, 2003. **115**(3): p. 255-66.
61. Atasoy, D., et al., *Deconstruction of a neural circuit for hunger.* Nature, 2012. **488**(7410): p. 172-7.

62. Garner, A.R., et al., *Generation of a synthetic memory trace.* Science, 2012. **335**(6075): p. 1513-6.
63. Tapken, D., et al., *A plant homolog of animal glutamate receptors is an ion channel gated by multiple hydrophobic amino acids.* Sci Signal, 2013. **6**(279): p. ra47.
64. Slimko, E.M., et al., *Selective electrical silencing of mammalian neurons in vitro by the use of invertebrate ligand-gated chloride channels.* J Neurosci, 2002. **22**(17): p. 7373-9.
65. Strader, C.D., et al., *Allele-specific activation of genetically engineered receptors.* J Biol Chem, 1991. **266**(1): p. 5-8.
66. Gao, Z.G., et al., *Orthogonal activation of the reengineered A3 adenosine receptor (neoceptor) using tailored nucleoside agonists.* J Med Chem, 2006. **49**(9): p. 2689-702.
67. Gomez, J.L., et al., *Chemogenetics revealed: DREADD occupancy and activation via converted clozapine.* Science, 2017. **357**(6350): p. 503-507.
68. Kandel, E.R., ed. *Principals of Neural Science*. 5th ed. 2013, McGraw-Hill: New York.
69. Acher, F.C. and H.O. Bertrand, *Amino acid recognition by Venus flytrap domains is encoded in an 8-residue motif.* Biopolymers, 2005. **80**(2-3): p. 357-66.
70. Turano, F.J., et al., *The putative glutamate receptors from plants are related to two superfamilies of animal neurotransmitter receptors via distinct evolutionary mechanisms.* Mol Biol Evol, 2001. **18**(7): p. 1417-20.
71. Lam, H.M., et al., *Glutamate-receptor genes in plants.* Nature, 1998. **396**(6707): p. 125-6.
72. Wudick, M.M., et al., *Comparing Plant and Animal Glutamate Receptors: Common Traits but Different Fates?* J Exp Bot, 2018.
73. Gradinaru, V., et al., *Molecular and cellular approaches for diversifying and extending optogenetics.* Cell, 2010. **141**(1): p. 154-165.
74. Isenberg, K.E. and G.E. Meyer, *Cloning of a putative neuronal nicotinic acetylcholine receptor subunit.* J Neurochem, 1989. **52**(3): p. 988-91.
75. Zheng, L., U. Baumann, and J.L. Reymond, *An efficient one-step site-directed and site-saturation mutagenesis protocol.* Nucleic Acids Res, 2004. **32**(14): p. e115.
76. Szobota, S., C. McKenzie, and H. Janovjak, *Optical control of ligand-gated ion channels.* Methods Mol Biol, 2013. **998**: p. 417-35.
77. Lin, C.Y., et al., *Enhancing Protein Expression in HEK-293 Cells by Lowering Culture Temperature.* PLoS One, 2015. **10**(4): p. e0123562.
78. Torashima, T., et al., *Lentivector-mediated rescue from cerebellar ataxia in a mouse model of spinocerebellar ataxia.* EMBO Rep, 2008. **9**(4): p. 393-9.
79. Biederer, T. and P. Scheiffele, *Mixed-culture assays for analyzing neuronal synapse formation.* Nat Protoc, 2007. **2**(3): p. 670-6.
80. Khom, S., et al., *Pharmacological properties of GABAA receptors containing gamma1 subunits.* Mol Pharmacol, 2006. **69**(2): p. 640-9.
81. Baburin, I., S. Beyl, and S. Hering, *Automated fast perfusion of Xenopus oocytes for drug screening.* Pflugers Arch, 2006. **453**(1): p. 117-23.
82. Khom, S., et al., *GABAA receptor modulation by piperine and a non-TRPV1 activating derivative.* Biochem Pharmacol, 2013. **85**(12): p. 1827-36.

83. Furukawa, H. and E. Gouaux, *Mechanisms of activation, inhibition and specificity: crystal structures of the NMDA receptor NR1 ligand-binding core.* EMBO J, 2003. **22**(12): p. 2873-85.
84. Traynelis, S.F., et al., *Glutamate receptor ion channels: structure, regulation, and function.* Pharmacol Rev, 2010. **62**(3): p. 405-96.
85. Petzoldt, A.G., et al., *Gating characteristics control glutamate receptor distribution and trafficking in vivo.* Curr Biol, 2014. **24**(17): p. 2059-65.
86. Qiu, S., et al., *An endoplasmic reticulum retention signal located in the extracellular amino-terminal domain of the NR2A subunit of N-Methyl-D-aspartate receptors.* J Biol Chem, 2009. **284**(30): p. 20285-98.
87. Diaz-Alonso, J., et al., *Subunit-specific role for the amino-terminal domain of AMPA receptors in synaptic targeting.* Proc Natl Acad Sci U S A, 2017. **114**(27): p. 7136-7141.
88. Lu, W. and K.W. Roche, *Posttranslational regulation of AMPA receptor trafficking and function.* Curr Opin Neurobiol, 2012. **22**(3): p. 470-9.
89. Fox, P.D., et al., *Induction of stable ER-plasma-membrane junctions by Kv2.1 potassium channels.* J Cell Sci, 2015. **128**(11): p. 2096-105.
90. Stern-Bach, Y., et al., *A point mutation in the glutamate binding site blocks desensitization of AMPA receptors.* Neuron, 1998. **21**(4): p. 907-18.
91. Yelshansky, M.V., et al., *Block of AMPA receptor desensitization by a point mutation outside the ligand-binding domain.* The Journal of neuroscience : the official journal of the Society for Neuroscience, 2004. **24**(20): p. 4728-36.
92. Kondoh, T., et al., *Lysine and arginine reduce the effects of cerebral ischemic insults and inhibit glutamate-induced neuronal activity in rats.* Front Integr Neurosci, 2010. **4**: p. 18.
93. Andine, P., et al., *Extracellular acidic sulfur-containing amino acids and gamma-glutamyl peptides in global ischemia: postischemic recovery of neuronal activity is paralleled by a tetrodotoxin-sensitive increase in cysteine sulfinate in the CA1 of the rat hippocampus.* Journal of neurochemistry, 1991. **57**(1): p. 230-6.
94. Lerma, J., et al., *In vivo determination of extracellular concentration of amino acids in the rat hippocampus. A method based on brain dialysis and computerized analysis.* Brain research, 1986. **384**(1): p. 145-55.
95. Yan, H., et al., *High-performance liquid chromatography method for determination of carnosic acid in rat plasma and its application to pharmacokinetic study.* Biomedical chromatography : BMC, 2009. **23**(7): p. 776-81.
96. Bergqvist, P.B., et al., *Brain extracellular quinolinic acid in chronic experimental hepatic encephalopathy as assessed by in vivo microdialysis: acute effects of L-tryptophan.* Neuropsychopharmacology : official publication of the American College of Neuropsychopharmacology, 1996. **15**(4): p. 382-9.
97. Yoshihara, S., et al., *Alterations in extracellular tryptophan and dopamine concentrations in rat striatum following peripheral administration of D- and L-tryptophan: an in vivo microdialysis study.* Neuroscience letters, 2012. **526**(1): p. 74-8.
98. Landolt, H., et al., *Extracellular antioxidants and amino acids in the cortex of the rat: monitoring by microdialysis of early ischemic changes.* Journal of cerebral blood flow and metabolism : official journal of the International Society of Cerebral Blood Flow and Metabolism, 1992. **12**(1): p. 96-102.

99. Andine, P., et al., *Intra- and extracellular changes of amino acids in the cerebral cortex of the neonatal rat during hypoxic-ischemia.* Brain research. Developmental brain research, 1991. **64**(1-2): p. 115-20.
100. Molchanova, S., et al., *Interstitial concentrations of amino acids in the rat striatum during global forebrain ischemia and potassium-evoked spreading depression.* Neurochemical research, 2004. **29**(8): p. 1519-27.
101. Jacobson, I., M. Sandberg, and A. Hamberger, *Mass transfer in brain dialysis devices--a new method for the estimation of extracellular amino acids concentration.* Journal of neuroscience methods, 1985. **15**(3): p. 263-8.
102. Zhang, D., et al., *Analysis of trace amino acid neurotransmitters in hypothalamus of rats after exhausting exercise using microdialysis.* Journal of chromatography. B, Biomedical sciences and applications, 2001. **758**(2): p. 277-82.
103. Farrant, M. and R.A. Webster, *Compartmental distribution of endogenous amino acids in the substantia nigra of the rat.* Brain research, 1989. **480**(1-2): p. 344-8.
104. Nakata, N., H. Kato, and K. Kogure, *Effects of repeated cerebral ischemia on extracellular amino acid concentrations measured with intracerebral microdialysis in the gerbil hippocampus.* Stroke, 1993. **24**(3): p. 458-63; discussion 463-4.
105. Nakata, N., H. Kato, and K. Kogure, *Ischemic tolerance and extracellular amino acid concentrations in gerbil hippocampus measured by intracerebral microdialysis.* Brain research bulletin, 1994. **35**(3): p. 247-51.
106. Glaeser, B.S., T.J. Maher, and R.J. Wurtman, *Changes in brain levels of acidic, basic, and neutral amino acids after consumption of single meals containing various proportions of protein.* J Neurochem, 1983. **41**(4): p. 1016-21.
107. Lada, M.W. and R.T. Kennedy, *In vivo monitoring of glutathione and cysteine in rat caudate nucleus using microdialysis on-line with capillary zone electrophoresis-laser induced fluorescence detection.* Journal of neuroscience methods, 1997. **72**(2): p. 153-9.
108. Twomey, E.C., et al., *Elucidation of AMPA receptor-stargazin complexes by cryo-electron microscopy.* Science, 2016. **353**(6294): p. 83-6.
109. Diaz, E., *Regulation of AMPA receptors by transmembrane accessory proteins.* Eur J Neurosci, 2010. **32**(2): p. 261-8.
110. Milstein, A.D. and R.A. Nicoll, *Regulation of AMPA receptor gating and pharmacology by TARP auxiliary subunits.* Trends Pharmacol Sci, 2008. **29**(7): p. 333-9.
111. Arellano, J.I., et al., *Ultrastructure of dendritic spines: correlation between synaptic and spine morphologies.* Front Neurosci, 2007. **1**(1): p. 131-43.
112. Harris, K.M. and J.K. Stevens, *Dendritic spines of CA 1 pyramidal cells in the rat hippocampus: serial electron microscopy with reference to their biophysical characteristics.* J Neurosci, 1989. **9**(8): p. 2982-97.
113. Petralia, R.S., *Distribution of extrasynaptic NMDA receptors on neurons.* ScientificWorldJournal, 2012. **2012**: p. 267120.
114. Keck, T., et al., *Synaptic scaling and homeostatic plasticity in the mouse visual cortex in vivo.* Neuron, 2013. **80**(2): p. 327-34.
115. Shipman, S.L., et al., *Distance-dependent scaling of AMPARs is cell-autonomous and GluA2 dependent.* J Neurosci, 2013. **33**(33): p. 13312-9.
116. Tchantchou, F., et al., *S-adenosylmethionine mediates glutathione efficacy by increasing glutathione S-transferase activity: implications for S-adenosyl*

methionine as a neuroprotective dietary supplement. J Alzheimers Dis, 2008. **14**(3): p. 323-8.
117. Werner, P., et al., *COMT-dependent protection of dopaminergic neurons by methionine, dimethionine and S-adenosylmethionine (SAM) against L-dopa toxicity in vitro.* Brain Res, 2001. **893**(1-2): p. 278-81.
118. Abi, I., R.A. Magaji, and M.G. Magaji, *Acute Administration of Methionine Affects Performance of Swiss Mice in Learning and Memory Paradigms.* Niger J Physiol Sci, 2015. **30**(1-2): p. 65-72.
119. Lee, J., H. Ryu, and N.W. Kowall, *Motor neuronal protection by L-arginine prolongs survival of mutant SOD1 (G93A) ALS mice.* Biochem Biophys Res Commun, 2009. **384**(4): p. 524-9.
120. Bowie, D., *Redefining the classification of AMPA-selective ionotropic glutamate receptors.* J Physiol, 2012. **590**(1): p. 49-61.
121. Stein, E.L. and D.M. Chetkovich, *Regulation of stargazin synaptic trafficking by C-terminal PDZ ligand phosphorylation in bidirectional synaptic plasticity.* J Neurochem, 2010. **113**(1): p. 42-53.
122. Hafner, A.S., et al., *Lengthening of the Stargazin Cytoplasmic Tail Increases Synaptic Transmission by Promoting Interaction to Deeper Domains of PSD-95.* Neuron, 2015. **86**(2): p. 475-89.
123. Tapken, D. and M. Hollmann, *Arabidopsis thaliana glutamate receptor ion channel function demonstrated by ion pore transplantation.* J Mol Biol, 2008. **383**(1): p. 36-48.
124. Hoffmann, J., et al., *Investigation via ion pore transplantation of the putative relationship between glutamate receptors and K+ channels.* Mol Cell Neurosci, 2006. **33**(4): p. 358-70.
125. Grange, E., et al., *Brain protein synthesis in the conscious rat using L-[35S]methionine: relationship of methionine specific activity between plasma and precursor compartment and evaluation of methionine metabolic pathways.* J Neurochem, 1992. **59**(4): p. 1437-43.
126. Alabi, A.A. and R.W. Tsien, *Synaptic vesicle pools and dynamics.* Cold Spring Harb Perspect Biol, 2012. **4**(8): p. a013680.
127. Takamori, S., et al., *Molecular anatomy of a trafficking organelle.* Cell, 2006. **127**(4): p. 831-46.
128. Sudhof, T.C., *The synaptic vesicle cycle.* Annu Rev Neurosci, 2004. **27**: p. 509-47.
129. Waites, C.L. and C.C. Garner, *Presynaptic function in health and disease.* Trends Neurosci, 2011. **34**(6): p. 326-37.
130. Kashani, A., et al., *Altered expression of vesicular glutamate transporters VGLUT1 and VGLUT2 in Parkinson disease.* Neurobiol Aging, 2007. **28**(4): p. 568-78.
131. Hirokawa, N., S. Niwa, and Y. Tanaka, *Molecular motors in neurons: transport mechanisms and roles in brain function, development, and disease.* Neuron, 2010. **68**(4): p. 610-38.
132. Arnold, S.E. and J.Q. Trojanowski, *Recent advances in defining the neuropathology of schizophrenia.* Acta Neuropathol, 1996. **92**(3): p. 217-31.
133. Mutch, S.A., et al., *Protein quantification at the single vesicle level reveals that a subset of synaptic vesicle proteins are trafficked with high precision.* J Neurosci, 2011. **31**(4): p. 1461-70.

134. Tabb, J.S., et al., *Glutamate transport into synaptic vesicles. Roles of membrane potential, pH gradient, and intravesicular pH.* J Biol Chem, 1992. **267**(22): p. 15412-8.
135. Naito, S. and T. Ueda, *Characterization of glutamate uptake into synaptic vesicles.* J Neurochem, 1985. **44**(1): p. 99-109.
136. Pereira, D.B., et al., *Fluorescent false neurotransmitter reveals functionally silent dopamine vesicle clusters in the striatum.* Nat Neurosci, 2016. **19**(4): p. 578-86.
137. Midorikawa, M. and T. Sakaba, *Imaging Exocytosis of Single Synaptic Vesicles at a Fast CNS Presynaptic Terminal.* Neuron, 2015. **88**(3): p. 492-8.
138. Rose, T., et al., *Developmental refinement of vesicle cycling at Schaffer collateral synapses.* Neuron, 2013. **77**(6): p. 1109-21.
139. Lee, M., et al., *Development of pH-responsive fluorescent false neurotransmitters.* J Am Chem Soc, 2010. **132**(26): p. 8828-30.
140. Vaithianathan, T., et al., *Nanoscale dynamics of synaptic vesicle trafficking and fusion at the presynaptic active zone.* Elife, 2016. **5**.
141. Herzog, E., et al., *In vivo imaging of intersynaptic vesicle exchange using VGLUT1 Venus knock-in mice.* J Neurosci, 2011. **31**(43): p. 15544-59.
142. Murthy, K., J.M. Bhat, and S.P. Koushika, *In vivo imaging of retrogradely transported synaptic vesicle proteins in Caenorhabditis elegans neurons.* Traffic, 2011. **12**(1): p. 89-101.
143. Panzer, J.A., Y. Song, and R.J. Balice-Gordon, *In vivo imaging of preferential motor axon outgrowth to and synaptogenesis at prepatterned acetylcholine receptor clusters in embryonic zebrafish skeletal muscle.* J Neurosci, 2006. **26**(3): p. 934-47.
144. Farsi, Z., et al., *Single-vesicle imaging reveals different transport mechanisms between glutamatergic and GABAergic vesicles.* Science, 2016. **351**(6276): p. 981-4.
145. Kwon, S.E. and E.R. Chapman, *Synaptophysin regulates the kinetics of synaptic vesicle endocytosis in central neurons.* Neuron, 2011. **70**(5): p. 847-54.
146. Alder, J., et al., *Overexpression of synaptophysin enhances neurotransmitter secretion at Xenopus neuromuscular synapses.* J Neurosci, 1995. **15**(1 Pt 2): p. 511-9.
147. Yao, J., et al., *Uncoupling the roles of synaptotagmin I during endo- and exocytosis of synaptic vesicles.* Nat Neurosci, 2011. **15**(2): p. 243-9.
148. Kahle, P.J., et al., *Subcellular localization of wild-type and Parkinson's disease-associated mutant alpha -synuclein in human and transgenic mouse brain.* J Neurosci, 2000. **20**(17): p. 6365-73.
149. Wang, Y.M., et al., *Knockout of the vesicular monoamine transporter 2 gene results in neonatal death and supersensitivity to cocaine and amphetamine.* Neuron, 1997. **19**(6): p. 1285-96.
150. de Castro, B.M., et al., *The vesicular acetylcholine transporter is required for neuromuscular development and function.* Mol Cell Biol, 2009. **29**(19): p. 5238-50.
151. Balschun, D., et al., *Vesicular glutamate transporter VGLUT1 has a role in hippocampal long-term potentiation and spatial reversal learning.* Cereb Cortex, 2010. **20**(3): p. 684-93.
152. Wojcik, S.M., et al., *A shared vesicular carrier allows synaptic corelease of GABA and glycine.* Neuron, 2006. **50**(4): p. 575-87.

153. Hua, Z., et al., *v-SNARE composition distinguishes synaptic vesicle pools.* Neuron, 2011. **71**(3): p. 474-87.
154. Kish, P.E. and T. Ueda, *Glutamate accumulation into synaptic vesicles.* Methods Enzymol, 1989. **174**: p. 9-25.
155. Roz, N., et al., *Inhibition of vesicular uptake of monoamines by hyperforin.* Life Sci, 2002. **71**(19): p. 2227-37.
156. Hu, K., et al., *Vesicular restriction of synaptobrevin suggests a role for calcium in membrane fusion.* Nature, 2002. **415**(6872): p. 646-50.
157. Reichhart, E., et al., *A Phytochrome Sensory Domain Permits Receptor Activation by Red Light.* Angew Chem Int Ed Engl, 2016. **55**(21): p. 6339-42.
158. Kehrl, J., et al., *Vesicular Glutamate Transporter Inhibitors: Structurally Modified Brilliant Yellow Analogs.* Neurochem Res, 2017. **42**(6): p. 1823-1832.
159. Venkatesan, S., et al., *Refinement of the Central Steps of Substrate Transport by the Aspartate Transporter GltPh: Elucidating the Role of the Na2 Sodium Binding Site.* PLoS Comput Biol, 2015. **11**(10): p. e1004551.
160. Nguyen, P.A., et al., *Using supported bilayers to study the spatiotemporal organization of membrane-bound proteins.* Methods Cell Biol, 2015. **128**: p. 223-241.
161. Ahmed, S., et al., *Small-scale isolation of synaptic vesicles from mammalian brain.* Nat Protoc, 2013. **8**(5): p. 998-1009.
162. Herculano-Houzel, S., B. Mota, and R. Lent, *Cellular scaling rules for rodent brains.* Proc Natl Acad Sci U S A, 2006. **103**(32): p. 12138-43.
163. Takamori, S., D. Riedel, and R. Jahn, *Immunoisolation of GABA-specific synaptic vesicles defines a functionally distinct subset of synaptic vesicles.* J Neurosci, 2000. **20**(13): p. 4904-11.
164. Gill, I., et al., *Presynaptic NMDA receptors - dynamics and distribution in developing axons in vitro and in vivo.* J Cell Sci, 2015. **128**(4): p. 768-80.
165. Schenck, S., et al., *Generation and Characterization of Anti-VGLUT Nanobodies Acting as Inhibitors of Transport.* Biochemistry, 2017. **56**(30): p. 3962-3971.
166. Pech, U., et al., *Optical dissection of experience-dependent pre- and postsynaptic plasticity in the Drosophila brain.* Cell Rep, 2015. **10**(12): p. 2083-95.
167. Zhu, Y., J. Xu, and S.F. Heinemann, *Two pathways of synaptic vesicle retrieval revealed by single-vesicle imaging.* Neuron, 2009. **61**(3): p. 397-411.
168. Campbell, R.E., et al., *A monomeric red fluorescent protein.* Proc Natl Acad Sci U S A, 2002. **99**(12): p. 7877-82.
169. Tarsa, L. and Y. Goda, *Synaptophysin regulates activity-dependent synapse formation in cultured hippocampal neurons.* Proc Natl Acad Sci U S A, 2002. **99**(2): p. 1012-6.
170. Fremeau, R.T., Jr., et al., *The expression of vesicular glutamate transporters defines two classes of excitatory synapse.* Neuron, 2001. **31**(2): p. 247-60.
171. Lodato, S., et al., *Excitatory projection neuron subtypes control the distribution of local inhibitory interneurons in the cerebral cortex.* Neuron, 2011. **69**(4): p. 763-79.
172. Attwell, D. and S.B. Laughlin, *An energy budget for signaling in the grey matter of the brain.* J Cereb Blood Flow Metab, 2001. **21**(10): p. 1133-45.
173. McIntire, S.L., et al., *Identification and characterization of the vesicular GABA transporter.* Nature, 1997. **389**(6653): p. 870-6.

174. Liu, Y., et al., *Preferential localization of a vesicular monoamine transporter to dense core vesicles in PC12 cells.* J Cell Biol, 1994. **127**(5): p. 1419-33.
175. Asanuma, M., et al., *Striatal astrocytes act as a reservoir for L-DOPA.* PLoS One, 2014. **9**(9): p. e106362.
176. Dieterich, D.C., et al., *In situ visualization and dynamics of newly synthesized proteins in rat hippocampal neurons.* Nat Neurosci, 2010. **13**(7): p. 897-905.
177. Li, L., et al., *Targeting tumor highly-expressed LAT1 transporter with amino acid-modified nanoparticles: Toward a novel active targeting strategy in breast cancer therapy.* Nanomedicine, 2017. **13**(3): p. 987-998.
178. Muller, J. and H. Heuer, *Expression pattern of thyroid hormone transporters in the postnatal mouse brain.* Front Endocrinol (Lausanne), 2014. **5**: p. 92.
179. Yanagida, O., et al., *Human L-type amino acid transporter 1 (LAT1): characterization of function and expression in tumor cell lines.* Biochim Biophys Acta, 2001. **1514**(2): p. 291-302.
180. del Amo, E.M., A. Urtti, and M. Yliperttula, *Pharmacokinetic role of L-type amino acid transporters LAT1 and LAT2.* Eur J Pharm Sci, 2008. **35**(3): p. 161-74.
181. Cestaro, B., *Effects of arginine, S-adenosylmethionine and polyamines on nerve regeneration.* Acta Neurol Scand Suppl, 1994. **154**: p. 32-41.
182. Roelcke, U., et al., *Alteration of blood-brain barrier in human brain tumors: comparison of [18F]fluorodeoxyglucose, [11C]methionine and rubidium-82 using PET.* J Neurol Sci, 1995. **132**(1): p. 20-7.
183. Boado, R.J., et al., *Site-directed mutagenesis of cysteine residues of large neutral amino acid transporter LAT1.* Biochim Biophys Acta, 2005. **1715**(2): p. 104-10.
184. Bik-Multanowski, M. and J.J. Pietrzyk, *LAT1 gene variants--potential factors influencing the clinical course of phenylketonuria.* J Inherit Metab Dis, 2006. **29**(5): p. 684.
185. Grewal, S., et al., *SNAT2 amino acid transporter is regulated by amino acids of the SLC6 gamma-aminobutyric acid transporter subfamily in neocortical neurons and may play no role in delivering glutamine for glutamatergic transmission.* J Biol Chem, 2009. **284**(17): p. 11224-36.
186. Armano, S., et al., *Localization and functional relevance of system a neutral amino acid transporters in cultured hippocampal neurons.* J Biol Chem, 2002. **277**(12): p. 10467-73.
187. Melone, M., et al., *Localization of the Na(+)-coupled neutral amino acid transporter 2 in the cerebral cortex.* Neuroscience, 2006. **140**(1): p. 281-92.
188. Banker, G.A. and W.M. Cowan, *Rat hippocampal neurons in dispersed cell culture.* Brain Res, 1977. **126**(3): p. 397-42.
189. Ono, M., et al., *Comparative evaluation of transport mechanisms of trans-1-amino-3-[(1)(8)F]fluorocyclobutanecarboxylic acid and L-[methyl-(1)(1)C]methionine in human glioma cell lines.* Brain Res, 2013. **1535**: p. 24-37.
190. Granger, A.J., M.L. Wallace, and B.L. Sabatini, *Multi-transmitter neurons in the mammalian central nervous system.* Curr Opin Neurobiol, 2017. **45**: p. 85-91.
191. Hnasko, T.S. and R.H. Edwards, *Neurotransmitter corelease: mechanism and physiological role.* Annu Rev Physiol, 2012. **74**: p. 225-43.
192. Zhang, S., et al., *Dopaminergic and glutamatergic microdomains in a subset of rodent mesoaccumbens axons.* Nat Neurosci, 2015. **18**(3): p. 386-92.
193. Aguilar, J.I., et al., *Neuronal Depolarization Drives Increased Dopamine Synaptic Vesicle Loading via VGLUT.* Neuron, 2017. **95**(5): p. 1074-1088 e7.

194. Hnasko, T.S., et al., *Vesicular glutamate transport promotes dopamine storage and glutamate corelease in vivo.* Neuron, 2010. **65**(5): p. 643-56.
195. Sames, D., et al., *Visualizing neurotransmitter secretion at individual synapses.* ACS Chem Neurosci, 2013. **4**(5): p. 648-51.
196. Tritsch, N.X., A.J. Granger, and B.L. Sabatini, *Mechanisms and functions of GABA co-release.* Nat Rev Neurosci, 2016. **17**(3): p. 139-45.
197. Jack, D.L., I.T. Paulsen, and M.H. Saier, *The amino acid/polyamine/organocation (APC) superfamily of transporters specific for amino acids, polyamines and organocations.* Microbiology, 2000. **146 (Pt 8)**: p. 1797-814.
198. Kutukova, E.A., et al., *The yeaS (leuE) gene of Escherichia coli encodes an exporter of leucine, and the Lrp protein regulates its expression.* FEBS Lett, 2005. **579**(21): p. 4629-34.
199. Liu, Q., et al., *YjeH Is a Novel Exporter of l-Methionine and Branched-Chain Amino Acids in Escherichia coli.* Appl Environ Microbiol, 2015. **81**(22): p. 7753-66.
200. Trotschel, C., et al., *Characterization of methionine export in Corynebacterium glutamicum.* J Bact, 2005. **187**(11): p. 3786-94.
201. Kadaba, N.S., et al., *The high-affinity E. coli methionine ABC transporter: structure and allosteric regulation.* Science, 2008. **321**(5886): p. 250-3.
202. Zimmermann, J., M.A. Herman, and C. Rosenmund, *Co-release of glutamate and GABA from single vesicles in GABAergic neurons exogenously expressing VGLUT3.* Front Synaptic Neurosci, 2015. **7**: p. 16.
203. Fu, Z., et al., *Functional excitatory synapses in HEK293 cells expressing neuroligin and glutamate receptors.* J Neurophysiol, 2003. **90**(6): p. 3950-7.
204. Scheiffele, P., et al., *Neuroligin expressed in nonneuronal cells triggers presynaptic development in contacting axons.* Cell, 2000. **101**(6): p. 657-69.
205. Urban, D.J. and B.L. Roth, *DREADDs (designer receptors exclusively activated by designer drugs): chemogenetic tools with therapeutic utility.* Annu Rev Pharmacol Toxicol, 2015. **55**: p. 399-417.
206. Michaelides, M., et al., *Whole-brain circuit dissection in free-moving animals reveals cell-specific mesocorticolimbic networks.* J Clin Invest, 2013. **123**(12): p. 5342-50.
207. Finkelstein, J.D. and J.J. Martin, *Homocysteine.* Int J Biochem Cell Biol, 2000. **32**(4): p. 385-9.
208. Obeid, R. and W. Herrmann, *Mechanisms of homocysteine neurotoxicity in neurodegenerative diseases with special reference to dementia.* FEBS Lett, 2006. **580**(13): p. 2994-3005.
209. Liu, L., W. Ito, and A. Morozov, *Overexpression of channelrhodopsin-2 interferes with the GABAb receptor-mediated depression of GABA release from the somatostatin-containing interneurons of the prefrontal cortex.* Neurophotonics, 2018. **5**(2): p. 025003.
210. Zimmermann, D., et al., *Effects on capacitance by overexpression of membrane proteins.* Biochem Biophys Res Commun, 2008. **369**(4): p. 1022-6.
211. Hippenmeyer, S., et al., *Genetic mosaic dissection of Lis1 and Ndel1 in neuronal migration.* Neuron, 2010. **68**(4): p. 695-709.
212. Kerr, J.N. and W. Denk, *Imaging in vivo: watching the brain in action.* Nature reviews. Neuroscience, 2008. **9**(3): p. 195-205.

213. Kosugi, A., et al., *MUP1, high affinity methionine permease, is involved in cysteine uptake by Saccharomyces cerevisiae.* Biosci Biotech Biochem, 2001. **65**(3): p. 728-31.